arXiv:2206.07731v1 [quant-ph] 15 Jun 2022

Controlling gain with loss: Bounds on localizable entanglement in multi-qubit systems

Jithin G. Krishnan, Harikrishnan K. J. and Amit Kumar Pal
Department of Physics, Indian Institute of Technology Palakkad, Palakkad 678 623, India
(Dated: June 17, 2022)

We investigate the relation between the amount of entanglement localized on a chosen subsystem of a multi-qubit system via local measurements on the rest of the system, and the bipartite entanglement that is lost during this measurement process. We study a number of paradigmatic pure states, including the generalized GHZ, the generalized W, Dicke, and the generalized Dicke states. For the generalized GHZ and W states, we analytically derive bounds on localizable entanglement in terms of the entanglement present in the system prior to the measurement. Also, for the Dicke and the generalized Dicke states, we demonstrate that with increasing system size, localizable entanglement tends to be equal to the bipartite entanglement present in the system over a specific partition before measurement. We extend the investigation numerically in the case of arbitrary multi-qubit pure states. We also analytically determine the modification of these results, including the proposed bounds, in situations where these pure states are subjected to single-qubit phase-flip noise on all qubits. Additionally, we study one-dimensional paradigmatic quantum spin models, namely the transverse-field XY model and the XXZ model in an external field, and numerically demonstrate a quadratic dependence of the localized entanglement on the lost entanglement. We show that this relation is robust even in the presence of disorder in the strength of the external field.

I. INTRODUCTION

In the last three decades, entanglement [1, 2] have been established as the key resource in quantum information processing tasks, including quantum teleportation [1, 3, 4], superdense coding [1, 5–7], and quantum cryptography [8, 9]. Concepts related to entanglement theory have also been used in areas that are seemingly different from quantum information theory, such as in probing gauge-gravity duality [10–13], in understanding time as an emergent phenomena from entanglement [14–16], and even in studying systems like photosynthetic complexes [17] that are important from biological point of view. These have motivated enormous experimental advancements in creating and manipulating entangled states in the laboratory using various substrates, namely, photons [18–20], trapped ions [21–23], cold atoms [24–26], superconducting qubits [27, 28], and nuclear magnetic resonance molecules [29]. Moreover, quantum many-body systems [30] have emerged as the natural choice for implementing quantum information processing tasks, and the necessity of studying the entanglement properties of these systems has also been realized [31, 32].

Entanglement over a subsystem A of a composite quantum system in the state ρ can be quantified by computing an appropriate entanglement measure E over the reduced state $\rho_A = \mathrm{Tr}_B[\rho]$ of the subsystem A, where B is the rest of the system [1, 2]. While this approach has been successful in a wide variety of multiparty quantum states [1, 2, 33], there exist states like N-qubit Greenberger-Horne-Zeilinger (GHZ) states [34], graph states [35], and stabilizer states in quantum error correcting codes [36, 37] for which the *partial trace-based* avenue may lead to vanishing entanglement measure on the state ρ_A. In such situations, one may take a *measurement-based* approach, where non-zero bipartite or multipartite entanglement can be *localized* on the subsystem A in the post-measured state of the system by performing measurements on B [38]. In the case of a multi-qubit system, this leads to the definition of the localizable entanglement [39–41], defined as the maximum average entanglement localized over A via local single-qubit projection measurements on all qubits in B, given by

$$\langle E_A\rangle = \max \sum_k p_k E(\tilde{\rho}_A^k). \tag{1}$$

Here, k labels the measurement outcomes corresponding to the post-measured states $\tilde{\rho}^k$ occurring with probability p_k ($\sum_k p_k = 1$), where $\tilde{\rho}_A^k = \mathrm{Tr}_B[\tilde{\rho}^k]$. Depending on the possible partitions in A, the entanglement measure E computed over A post-measurement can be either a bipartite [39–41], or a multipartite [42] measure. Apart from successfully characterizing entanglement in GHZ and GHZ-like states such as the graph [35] and the stabilizer states [43, 44], localizable entanglement and related ideas have been immensely useful in defining the correlation length in one-dimensional (1D) quantum spin models [39–41, 45], in characterizing quantum phase transitions in the cluster-Ising [46, 47] and cluster-XY models [48] in terms of entanglement, and in entanglement percolation through quantum networks [49].

The measurement on the subsystem B completely decouples B from A, leading to

$$\rho \to \tilde{\rho} = \tilde{\rho}_A \otimes \tilde{\rho}_B, \tag{2}$$

implying a complete loss in entanglement over all qubits belonging to the different subsystems A and B. A natural question that arises is *whether and how the entanglement $\langle E_A\rangle$ localized on A via measurements on B depends on the entanglement that is lost during the same measurement process*. More specifically, considering a bipartition $A_1 : A_2$ of A (i.e., an overall tripartition $A_1 : A_2 : B$ of the multi-qubit system, see Fig. 1), and a bipartite entanglement measure E, we ponder on the following question: *Does any relation exist between the bipartite entanglement $\langle E_A\rangle \equiv \langle E_{A_1A_2}\rangle$ localized over the subsystem A via single-qubit projection measurements on all qubits in B, and the entanglement over different bipartitions prior to the measurement, namely, $E_{A_1A_2:B}$, $E_{A_1:A_2B}$, and $E_{A_2:A_1B}$, that are lost during the measurement process leading to $\langle E_{A_1A_2}\rangle$?* On one hand, answer to this question may give rise to constraints on the entanglement localizable over

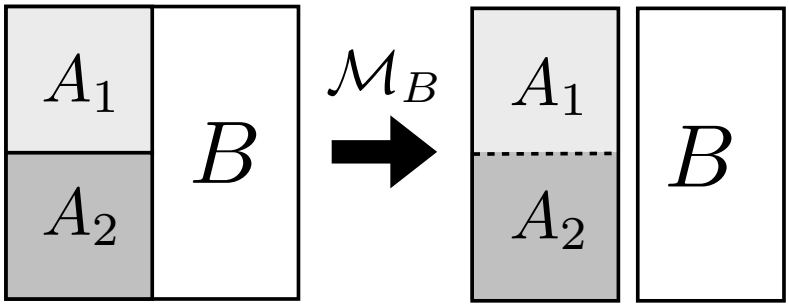


FIG. 1. Consider a multi-qubit system divided into three subsystems, A_1, A_2, and B, with bipartite entanglement $E_{A_1A_2:B}$, $E_{A_1:A_2B}$, and $E_{A_2:A_1B}$ over different bipartitions. Measurement on all qubits in B, denoted by $\mathcal{M}_B$, decouples the subsystem B from the qubits in $A \equiv A_1A_2$.

the subsystem of a multi-qubit system in terms of the entanglement present in the system prior to measurement – a situation that is of fundamental interest from the perspective of complete characterization of the system via entanglement. On the other hand, such a study may also aid in estimating the localizable entanglement prior to the measurement via the information on the bipartite entanglement present in the system. The latter is advantageous from a practical point of view, specially in situations where performing the measurements and optimizing over all possible measurements may turn out to be difficult.

A few results exist in this direction. Note that the monotonicity of E [1, 33, 50–52] implies that

$$\langle E_{A_1A_2}\rangle \leq \min\left[E_{A_1:A_2B}, E_{A_2:A_1B}\right]. \tag{3}$$

It has been shown that the inequality (3) can be tightened to an equality in the case of asymptotic pure state distillation [53, 54]. At the single copy level, it has also been shown that for all three-qubit pure states with each of A_1, A_2, and B being a qubit, the inequality (3) becomes an equality via some measurement on B for a specific choice of entanglement measure [55]. In the case of multi-qubit pure states, investigation on the relation between localizable multipartite entanglement $\langle E_A\rangle$ and the multipartite entanglement, as quantified by the multiparty entanglement measure E, over the state prior to the measurement has also been made [42]. However, we are still far from a systematic and complete understanding of the problem in the case of arbitrary multi-qubit quantum states.

In this paper, we study the interplay between $\langle E_{A_1A_2}\rangle$, $E_{A_1:A_2B}$, $E_{A_2:A_1B}$, and $E_{A_1A_2:B}$ in multi-qubit systems, where each of the partitions A_1, A_2, and B may consist of multiple qubits, choosing negativity [56–60] as the entanglement measure. We start with the investigation of a number of paradigmatic N-qubit pure states, including the generalized GHZ states [34, 61], the generalized W states [61, 62], Dicke states [63–66], and generalized Dicke states [42], and analytically derive bounds of $\langle E_{A_1A_2}\rangle$ in terms of $E_{A_1:A_2B}$, $E_{A_2:A_1B}$, and $E_{A_1A_2:B}$. In the cases of arbitrary pure states of N-qubits, we numerically investigate whether it is always possible to exceed the loss in bipartite entanglement via localization performed through measurement. We extend our investigation to the pure states subjected to the single-qubit phase flip noise [67, 68] of Markovian [69] and non-Markovian [70–72] type, and discuss the modifications of the bounds obtained for pure states due to the presence of noise. We also look into the ground states obtained from one-dimensional (1D) interacting quantum spin models, both in the presence and absence of disorder [73]. More specifically, we consider the 1D transverse-field XY model [74–79] and the 1D XXZ model in an external field [80–85], where disorder can be present in the strength of the field. We numerically demonstrate a quadratic dependence of the localizable entanglement on the entanglement lost during measurement in the ground states of the ordered and the disordered models, and demonstrate that the relation is robust against the presence of disorder in the field-strength.

The rest of the paper is organized as follows. In Sec. II, we formally define the localizable entanglement, and compute it, along with the bipartite entanglements present in the unmeasured states, in the case of paradigmatic multi-qubit pure states. We also present the numerical data corresponding to arbitrary N-qubit pure states, and discuss the implications of the data. The modifications of the results for the pure state due to subjecting the states to single-qubit Markovian and non-Markovian phase flip channels are discussed in Sec. III. The study of the localizable and the lost entanglement in the ground states of ordered and disordered 1D quantum spin models can be found in Sec. IV. Sec. V presents the outlook and concluding remarks.

II. MULTI-QUBIT PURE STATES

In this section, we consider a number of paradigmatic multi-qubit pure states, and investigate the possible correlation between the localizable entanglement and the bipartite entanglement that is lost due to measurement. Note that the maximum value of $\langle E_{A_1A_2}\rangle$ as well as the optimal measurement basis on B providing this value depends on the choice of E. For the results reported in this paper, we choose negativity [56–60] as the entanglement measure. See Appendix A for a brief definition.

Let us consider an N-qubit system, S, where the qubits are labelled as $1, 2, \cdots, N$. As discussed in Sec. I, we consider a tripartition $A_1 : A_2 : B$ of the system, and perform single-qubit rank-1 projection measurements on all qubits in B. With-

out any loss in generality, we assume that B holds $n(< N-1)$ qubits, and $A = A_1 \cup A_2$ consists of the rest $N-n$ qubits. We label the qubits in B as $1, 2, \cdots, n$, and the qubits in A as $n+1, n+2, \cdots, N-1, N$. In this situation, $\langle E_{A_1A_2}\rangle$ (Eq. 1) takes the form

$$\langle E_{A_1A_2}\rangle = \max \sum_{k=0}^{2^n-1} p_k E(\tilde{\rho}^k_{A_1A_2}), \tag{4}$$

where $\tilde{\rho}^k_{A_1A_2} = \mathrm{Tr}_B\left[\tilde{\rho}^k\right]$, $\tilde{\rho}^k = \left[M^k \rho M^{k\dagger}\right]/p_k$, and $p_k = \mathrm{Tr}\left[M^k \rho M^{k\dagger}\right]$, with M^k being the measurement operation corresponding to the measurement outcome k, and the maximization is performed over the set of all possible single-qubit rank-1 projection measurements on all qubits in B. Note that the maximum value of $\langle E_{A_1A_2}\rangle$ can not exceed the maximum value of the chosen entanglement measure, E_{max}, implying $\langle E_{A_1A_2}\rangle \leq E_{max}$.

The measurement operators $\{M^k\}$ can be written as $M^k = I_{A_1A_2} \otimes P^k_B$, with the projectors on the qubits in B corresponding to the measurement outcome k given by $P^k_B = |\tilde{b}_k\rangle\langle\tilde{b}_k|$, where $k_i = 0, 1$ and $k \equiv k_1 k_2 \cdots k_n$ is a multi-index. Here, $|\tilde{b}_k\rangle = \otimes_{\forall i \in B} |b_{k_i}\rangle$, and

$$\begin{aligned} |b_0\rangle_i &= \cos\frac{\theta_i}{2}|0\rangle + e^{i\phi_i}\sin\frac{\theta_i}{2}|1\rangle, \\ |b_1\rangle_i &= \sin\frac{\theta_i}{2}|0\rangle - e^{i\phi_i}\cos\frac{\theta_i}{2}|1\rangle, \end{aligned} \tag{5}$$

on all qubits $i \in B$, where $\theta_i, \phi_i \in \mathbb{R}$, $0 \leq \theta_i \leq \pi$, $0 \leq \phi \leq 2\pi$. Unless otherwise stated, we maintain these notations in all subsequent calculations. Also, we use A and A_1A_2 interchangeably, since $A \equiv A_1 \cup A_2 = A_1A_2$.

A. Generalized GHZ states

We start with the N-qubit generalized GHZ (gGHZ) state [34], given by

$$|\,\mathrm{gGHZ}\rangle = a_0|0\rangle^{\otimes N} + a_1|1\rangle^{\otimes N}, \tag{6}$$

where a_0 and a_1 are complex numbers, i.e., $a_0, a_1 \in \mathbb{C}$, and the state is normalized, implying $|a_0|^2 + |a_1|^2 = 1$. For the gGHZ state, we present the following proposition.

■ **Proposition I.** *For any tripartition $A_1 : A_2 : B$ of an N-qubit gGHZ state,*

$$\langle E_{A_1A_2}\rangle = E_{A_1A_2:B} = E_{A_1:A_2B} = E_{A_2:A_1B}. \tag{7}$$

Proof. Partial transposition of $\rho = |\,\mathrm{gGHZ}\rangle\langle\mathrm{gGHZ}|$ with respect to the subsystems B leads to

$$\begin{aligned} \rho^{T_B} = &|a_0|^2(|0\rangle\langle 0|)^{\otimes N} + |a_1|^2(|1\rangle\langle 1|)^{\otimes N} \\ &+a_0a_1^*(|0\rangle\langle 1|)^{\otimes N-n}(|1\rangle\langle 0|)^{\otimes n} \\ &+a_0^*a_1(|1\rangle\langle 0|)^{\otimes N-n}(|0\rangle\langle 1|)^{\otimes n}, \end{aligned} \tag{8}$$

with non-zero eigenvalues $|a_0|^2, |a_1|^2, \pm|a_0||a_1|$. Therefore the entanglement between partition A_1A_2 and partition B, as quantified by negativity, is given by

$$E_{A_1A_2:B} = 2|a_0|\sqrt{1-|a_0|^2}. \tag{9}$$

We now compute localizable entanglement, $\langle E_{A_1A_2}\rangle$, for the gGHZ state. Application of the measurement operator M^k corresponding to the measurement outcome k on $|\,\mathrm{gGHZ}\rangle$ leads to

$$M^k|\,\mathrm{gGHZ}\rangle = |\,\mathrm{gGHZ}_k\rangle_{A_1A_2} \otimes |\tilde{b}_k\rangle_B \tag{10}$$

where

$$\begin{aligned} |\,\mathrm{gGHZ}_k\rangle &= \frac{1}{\sqrt{p_k}}\left(a_0 f_0^k|0\rangle^{\otimes n} + a_1 f_1^k|1\rangle^{\otimes n}\right), \\ p_k &= |a_0|^2|f_0^k|^2 + |a_1|^2|f_1^k|^2. \end{aligned} \tag{11}$$

Here,

$$\begin{aligned} f_0^k &= \prod_{i\in B} f_0^{k_i} = \prod_{i\in B}\langle b_{k_i}|0\rangle_i, \\ f_1^k &= \prod_{i\in B} f_1^{k_i} = \prod_{i\in B}\langle b_{k_i}|1\rangle_i \end{aligned} \tag{12}$$

are functions of $2n$ real parameters $\{\theta_i, \phi_i\}$, $i = 1, \cdots, n$. The negativity, $E^k_{A_1:A_2}$, can now be computed for each post-measured states $|\,\mathrm{gGHZ}_k\rangle$ on A_1A_2 as

$$E^k_{A_1:A_2} = \frac{2|a_0|\sqrt{1-|a_0|^2}|f_0^k||f_1^k|}{p_k}. \tag{13}$$

The localizable entanglement across the bipartition $A_1 : A_2$ of A is, therefore,

$$\langle E_{A_1:A_2}\rangle = 2|a_0|\sqrt{1-|a_0|^2}\left[\max\sum_{k=0}^{2^n-1}|f_0^k||f_1^k|\right]. \tag{14}$$

In order to perform the maximization, we note that $|f^k_{0,1}|$, and subsequently p_k and $E^k_{A_1:A_2}$, are independent of $\{\phi_i\}$, $i = 1, \cdots, n$, thereby reducing the maximization problem to one involving n real parameters, $\{\theta_i\}$, $i = 1, \cdots, n$. Moreover, since $|f^k_{0,1}| \geq 0$, and

$$|f_0^k||f_1^k| = \frac{1}{2^n}\prod_{\forall i\in B}\sin\theta_i, \tag{15}$$

one obtains

$$\begin{aligned} \max_{\theta_i}\sum_{k=0}^{2^n-1}|f_0^k||f_1^k| &= \frac{1}{2^n}\sum_{k=0}^{2^n-1}\max_{\theta_i}\prod_{\forall i\in B}\sin\theta_i \\ &= 1, \end{aligned} \tag{16}$$

where the maximization takes place for $\theta_i = \frac{\pi}{2}$ $\forall i \in B$, implying that a σ^x measurement on all qubits in B is optimal for obtaining the maximum $\langle E_{A_1A_2}\rangle$ as

$$\langle E_{A_1A_2}\rangle = 2|a_0|\sqrt{1-|a_0|^2}. \tag{17}$$

It is easy to see from the symmetry of the gGHZ state that $E_{A_1A_2:B} = E_{A_1:A_2B} = E_{A_2:A_1B}$, leading to

$$\langle E_{A_1A_2}\rangle = E_{A_1A_2:B} = E_{A_1:A_2B} = E_{A_2:A_1B}. \tag{18}$$

Hence the proof. □

Therefore, in the case of the N-qubit gGHZ states, it is not possible to exceed the bipartite entanglement present in the state prior to the measurement via localizable entanglement. Note also that for the N-qubit gGHZ state, (3) is an equality.

B. Generalized W states

Next, we focus on the N-qubit generalized W states [61, 62], given by

$$|\,\mathrm{gW}\rangle = \sum_{i=1}^{N} a_i \,|0\rangle^{\otimes(i-1)} \,|1\rangle_i \,|0\rangle^{\otimes(N-i)}\,, \tag{19}$$

where $a_i \in \mathbb{C}\ \forall i \in \{1,2,\cdots,N\}$, satisfying the normalization condition $\sum_{i=1}^{N}|a_i|^2 = 1$. Let us first consider a subset of the N-qubit gW states given in Eq. (19) where the coefficients a_i are real, i.e., $a_i \in \mathbb{R}$. We first focus on the correlation between $\langle E_{A_1A_2}\rangle$ and $E_{A_1A_2:B} \equiv E_{AB}$. Negativity over any bipartition AB of the system is given by[1]

$$E_{A_1A_2:B} = 2\left|\left[\left(\sum_{i=n+1}^{n+m} a_i^2 + \sum_{i=n+m+1}^{N} a_i^2\right)\sum_{i=1}^{n} a_i^2\right]^{\frac{1}{2}}\right|, \tag{20}$$

where we have assumed that qubits $1,2,\cdots,n$ constitute the subsystem B, and qubits $n+1,n+2,\cdots,N$ form the subsystem B. On the other hand, computation of $\langle E_{A_1A_2}\rangle$ involves application of M^k, $k=0,1,\cdots,2^n-1$, on the n qubits in B of $|\,\mathrm{gW}\rangle$ (see Sec. II A), leading to

$$M^k|\,\mathrm{gW}\rangle = |\tilde{b}_k\rangle_B \otimes |\psi_k\rangle_{A_1A_2} \tag{21}$$

with

$$|\psi_k\rangle = c_0^k\,|0\rangle^{\otimes(N-n)} + \sum_{i=1}^{N-n} c_i^k\,|0\rangle^{\otimes(i-1)}\,|1\rangle_i\,|0\rangle^{\otimes(N-n-i)}\,, \tag{22}$$

where $c_0^k = f_0^k/\sqrt{p_k}$, and $c_i^k = f_i^k/\sqrt{p_k}$, $i=1,2,\cdots,n$, with p_k being the probability of obtaining the measurement outcome k, such that $\sum_{i=0}^{N-n}|c_i^k|^2 = 1$, ensuring normalization. Note further that among the coefficients c_i^k, $i = 0,1,\cdots,N-n$, only c_0^k is complex (see Appendix B for explicit examples with the cases of single- and two-qubit measurements). Using this, and writing negativity in the state $|\psi_k\rangle$ over the bipartition $A_1:A_2$ can be written for all k as[2]

$$E^k_{A_1A_2} = 2\left|\left[\left(\sum_{i=n+1}^{n+m} a_i^2\right)\sum_{n+m+1}^{N} a_i^2\right]^{\frac{1}{2}}\right|. \tag{23}$$

[1] For gW states with real coefficients, this can be obtained by observing the patterns of the negative eigenvalues of the partially transposed density matrix of the smaller systems. Eq. (20) is also verified numerically for large gW states with real coefficients as well as complex coefficients, where in the case of the latter, a_i^2 is replaced with $|a_i|^2$.

[2] For gW states with real coefficients, this can be obtained following the same approach as for Eq. (20). For gW states with complex coefficients, a_i^2s are replaced by $|a_i|^2$s.

Here, we have assumed, without any loss in generality, that the subsystem A_1 (A_2) is constituted of the qubits $n+1,n+2,\cdots,n+m$ (qubits $n+m+1,n+m+2,\cdots,N$). Since $E_{A_1A_2} = E(\tilde{\rho}^k_{A_1A_2})$ is independent of θ,ϕ, localizable entanglement over the subsystem $A \equiv A_1A_2$ is given by

$$\langle E_{A_1A_2}\rangle = E^k_{A_1A_2} \tag{24}$$

We now propose the following for an N-qubit gW state with real coefficients.

■ **Proposition II.** *In the space $(E_{A_1A_2:B}, \langle E_{A_1A_2}\rangle)$, the localizable entanglement $\langle E_{A_1A_2}\rangle$ of an N-qubit normalized gW state with real coefficients is upper bounded by the line*

$$\langle E_{A_1A_2}\rangle = \frac{1}{2}\left(1+\sqrt{1-E^2_{A_1A_2:B}}\right), \tag{25}$$

where $E_{A_1A_2:B}$ is the bipartite entanglement over the bipartition $A_1A_2 : B$ in the state prior to measurement on all the qubits in B.

Proof. For ease of calculation, we focus on $\langle E_{A_1A_2}\rangle^2$ given by (using Eq. (23) and normalization of the gW state)

$$\langle E_{A_1A_2}\rangle^2 = 4\left(1-\sum_{i=1}^{n} a_i^2 - \sum_{i=n+1}^{n+m} a_i^2\right)\sum_{i=n+1}^{n+m} a_i^2, \tag{26}$$

which, for fixed $a = \sum_{i=1}^{n} a_i^2$, is a single-parameter function $F(x) = 4x(1-a-x)$ of x, where $x \equiv \sum_{i=n+1}^{n+m} a_i^2$. The function $F(x)$ has the maximum value $(1-a)^2$, occurring at $x = (1-a)/2$. This implies $\sum_{i=n+1}^{n+m} a_i^2 = (1-a)/2$ for the maximum of $\langle E_{A_1A_2}\rangle = 1-a$. Note also from Eq. (20) that $E_{A_1A_2:B} = 2\sqrt{a(1-a)}$. Eliminating a and subsequently solving for $\langle E_{A_1A_2}\rangle$, one obtains Eq. (25). □

The following Corollaries can be obtained straightforwardly from Proposition I.

◇ **Corollary II.1.** *The family of gW states with real coefficients that satisfy Eq. (25) are given by*

$$\sum_{i=n+1}^{n+m} a_i^2 = \sum_{i=n+m+1}^{N} a_i^2 = \frac{1}{2}\left(1-\sum_{i=1}^{n} a_i^2\right). \tag{27}$$

Proof. For a fixed value of $\sum_{i=1}^{n} a_i^2$, the maximization condition for $\langle E_{A_1A_2}\rangle$ is given by $\sum_{i=n+1}^{n+m} a_i^2 = \frac{1}{2}\left(1-\sum_{i=1}^{n} a_i^2\right)$. From the normalization of the gW states, Eq. (27) follows. □

◇ **Corollary II.2.** *For the family of gW states given by Eq. (27), $E_{A_1:A_2B} = E_{A_2:A_1B}$.*

Proof. Similar to Eq. (20), entanglement over the bipartitions $A_2 : A_1B$ and $A_1 : A_2B$ can be written as

$$E_{A_1:A_2B} = 2\left|\left[\left(\sum_{i=1}^{n} a_i^2 + \sum_{i=n+m+1}^{N} a_i^2\right)\sum_{i=n+1}^{n+m} a_i^2\right]^{\frac{1}{2}}\right|, \tag{28}$$

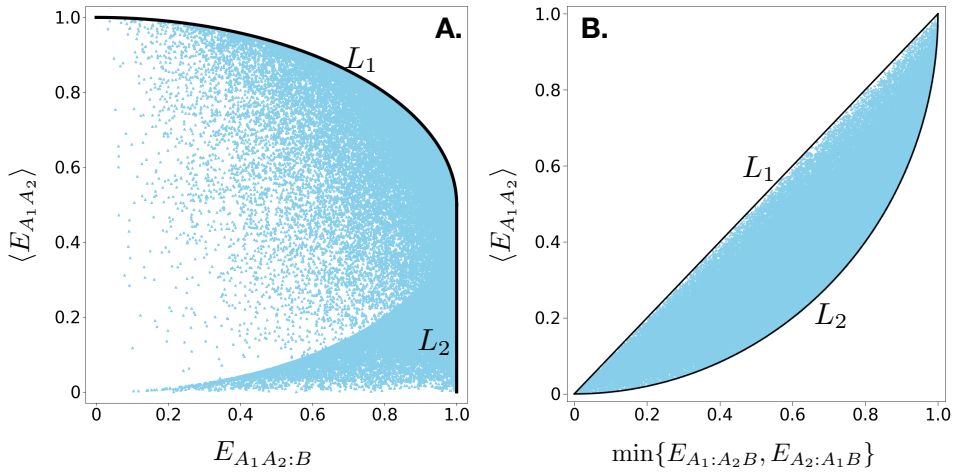


FIG. 2. **Generalized W states.** Scatter plot of a sample of 10^7 Haar-uniformly generated 3-qubit gW states on the **A.** $(E_{A_1A_2:B}, \langle E_{A_1A_2}\rangle)$ plane and the **B.** $(\min\{E_{A_1:A_2B}, E_{A_2:A_1B}\}, \langle E_{A_1A_2}\rangle)$ plane. The lines L_1 and L_2 on the $(E_{A_1A_2:B}, \langle E_{A_1A_2}\rangle)$ plane represent respectively the family of states following Eq. (25), and $E_{A_1A_2:B} = 1$. On the other hand, the lines L_1 and L_2 on the $(\min\{E_{A_1:A_2B}, E_{A_2:A_1B}\}, \langle E_{A_1A_2}\rangle)$ plane represent the family of states obeying Eqs. (30) and (31) respectively. All the axes in all figures are dimensionless.

and

$$E_{A_2:A_1B} = 2\left|\left[\left(\sum_{i=1}^{n} a_i^2 + \sum_{i=n+1}^{n+m} a_i^2\right)\sum_{i=n+m+1}^{N} a_i^2\right]^{\frac{1}{2}}\right|, \tag{29}$$

respectively. Clearly, for $\sum_{i=n+1}^{n+m} a_i^2 = \sum_{i=n+m+1}^{N} a_i^2$, $E_{A_1:A_2B} = E_{A_2:A_1B}$. □

■ **Proposition III.** *In* $(\min\{E_{A_1:A_2B}, E_{A_2:A_1B}\}, \langle E_{A_1A_2}\rangle)$ *space, the localizable entanglement* $\langle E_{A_1A_2}\rangle$ *of an* N*-qubit normalized gW state with real coefficients is upper-bounded by the line*

$$\langle E_{A_1A_2}\rangle = \min\{E_{A_1:A_2B}, E_{A_2:A_1B}\}, \tag{30}$$

and lower-bounded by the line

$$\langle E_{A_1A_2}\rangle^2 - 2\langle E_{A_1A_2}\rangle + (\min\{E_{A_1:A_2B}, E_{A_2:A_1B}\})^2 = 0, \tag{31}$$

where $E_{A_1:A_2B}$ $(E_{A_2:A_1B})$ *is the bipartite entanglement over the bipartition* $A_1 : A_2B$ $(A_2 : A_1B)$ *in the state prior to measurement on all the qubits in* B.

Proof. The upper bound follows from the monotonicity of E (see Eq. (3)). On the other hand, note that from Eqs. (28) and (29),

$$E_{A_1:A_2B}^2 = 4\left(\sum_{i=n+1}^{n+m} a_i^2\right)\sum_{i=1}^{n} a_i^2 + \langle E_{A_1A_2}\rangle^2, \tag{32}$$

and

$$E_{A_2:A_1B}^2 = 4\left(\sum_{i=n+m+1}^{N} a_i^2\right)\sum_{i=1}^{n} a_i^2 + \langle E_{A_1A_2}\rangle^2, \tag{33}$$

respectively, where we have used Eqs. (23) and (24). Let us proceed by assuming $E_{A_2:A_1B} \geq E_{A_1:A_2B}$, implying $\min\{E_{A_1:A_2B}, E_{A_2:A_1B}\} = E_{A_1:A_2B}$, and $\sum_{i=n+m+1}^{N} a_i^2 \geq \sum_{i=n+1}^{n+m} a_i^2$. For a fixed $a = \sum_{i=n+1}^{n+m} a_i^2$, $\langle E_{A_1A_2}\rangle$ is minimum if $\sum_{i=n+m+1}^{N} a_i^2$ is minimum, leading to $\sum_{i=n+m+1}^{N} a_i^2 = a$, and subsequently $\langle E_{A_1A_2}\rangle \geq 2a$ and $E_{A_1:A_2B} = 2\sqrt{a(1-a)}$. Eliminating a, we obtain the equation of the lower bound as

$$\langle E_{A_1A_2}\rangle^2 - 2\langle E_{A_1A_2}\rangle + E_{A_1:A_2B}^2 = 0. \tag{34}$$

Similarly, assuming $E_{A_1:A_2B} \geq E_{A_2:A_1B}$, one can also prove that

$$\langle E_{A_1A_2}\rangle^2 - 2\langle E_{A_1A_2}\rangle + E_{A_2:A_1B}^2 = 0. \tag{35}$$

Eqs. (34) and (35) lead to Eq. (31). □

Note 1. Note here that Propositions II and III, and the related Corollaries are proved for the subclass of gW states with real coefficients, and it is therefore logical to ask whether the same results apply to the three-qubit gW states with complex coefficients. While analytical calculation is difficult for a generic N-qubit gW state due to increase in the number of state parameters, we numerically check the applicability of these results for N-qubit gW states with complex coefficients, and find them to be valid. Therefore, for generic gW states, Propositions II, III, and Corollaries II.1 and II.2 can be straightforwardly updated by replacing a_i^2 with $|a_i|^2$ for all $i = 1, \cdots, N$. For demonstrations of these results, see Figs. 2A-B. Specific examples of the family of states described in Eq. (27) can be found in Appendix C.

Note 2. Note in Fig. 2A that apart from the line given by Eq. (25), the Haar uniformly [86, 87] chosen gW states are also bounded by the lines (a) $E_{A_1A_2:B} = 0$, (b) $\langle E_{A_1A_2}\rangle = 0$, and (c) $E_{A_1A_2:B} = 1$, which are not shown explicitly in the figure, and which are obtained from the fact that $0 \leq E_{A_1A_2:B}, \langle E_{A_1A_2:B}\rangle \leq 1$. It is worthwhile to note that the

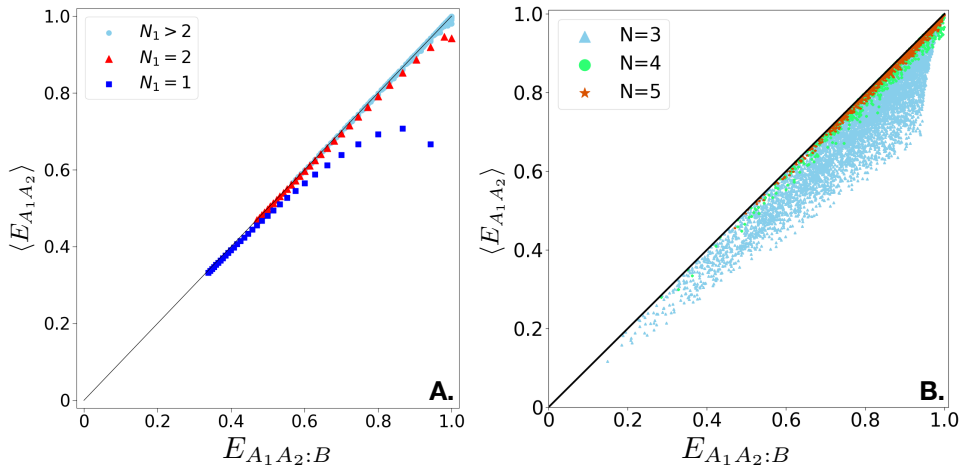


FIG. 3. **Dicke states. A.** Scatter plots of $|D(N, N_1)\rangle$ for $N \leq 35$ on the $(E_{A_1A_2:B}, \langle E_{A_1A_2} \rangle)$ plane, with all possible values of $N_1 = 1, \cdots, N-1$. **B.** Scatter plot of Haar-uniformly generated gD states of $N = 3$, $N = 4$, and $N = 5$ qubits on the $(E_{A_1A_2:B}, \langle E_{A_1A_2} \rangle)$ plane, where each of the subsystems B and A_1 is constituted of one qubit only. For each value of N, a sample of 10^5 states are used. All the axes in all figures are dimensionless.

family of gW states, for which $E_{A_1A_2:B} = 1$, are given by

$$4\sum_{i=1}^{n} a_i^2 = 1/\sum_{i=n+1}^{N} a_i^2. \tag{36}$$

The significance of these states will be clear in Sec. III B. For examples of such states, see Appendix C.

C. Dicke states

We now consider the class of *symmetric* states that remain invariant under permutation of parties. More specifically, we focus on the Dicke states [63–66] of N-qubits, where N_0 qubits are in the ground state $|0\rangle$, and the rest $N_1 = N - N_0$ qubits are in the excited state $|1\rangle$. A Dicke state with N_1 excited qubits can be written as

$$|D(N, N_1)\rangle = \frac{1}{\sqrt{\binom{N}{N_1}}} \sum_i \mathcal{P}_i \left(|0\rangle^{\otimes N-N_1} |1\rangle^{\otimes N_1} \right), \tag{37}$$

where for a fixed N, $N_1 = 0, 1, 2, \cdots, N$. Here, $\{\mathcal{P}_i\}$ is the set of all possible permutations of N_0 (N_1) qubits at ground (excited) state, such that $N_0 + N_1 = N$. Note that $|D(N, 0)\rangle$ and $|D(N, N)\rangle$ are product states, while $|D_1\rangle$ and $|D_{N-1}\rangle$ are identical to N-qubit W states, or its local unitary equivalents, the results for which can be determined as special cases of the gW states discussed in Sec. II B. Note also that in the case of $n = m < N/2$ ($n = m < (N-1)/2$) where N is even (odd), with m being the size of the subsystem A_1, symmetry of the Dicke states under qubit permutations suggests that $E_{A_1:A_2B} = E_{A_1A_2:B}$. We focus on the scenario where $n = 1$, and without any loss in generality, measure on qubit 1. Negativity for Dicke states are computable over 1:rest bipartition as [88] (see also [89, 90])

$$E_{A_1A_2:B} = \max_{i,j,i\neq j} \frac{1}{\binom{N}{N_1}} \sqrt{\binom{N-1}{N_1-i}\binom{N-1}{N_1-j}}, \tag{38}$$

where B is constituted of one (measured) qubit, and $i, j = 0, 1$.

In the case of $|D(N, N_1)\rangle$, the normalized post-measured states are given by

$$|D\rangle = \frac{1}{\sqrt{p}} \Big[\sqrt{\frac{N-N_1}{N}} \cos\frac{\theta}{2} D(N-1, N_1) + \sqrt{\frac{N_1}{N}} e^{-i\phi} \sin\frac{\theta}{2} D(N-1, N_1-1) \Big], \tag{39}$$

$$|D_\perp\rangle = \frac{1}{\sqrt{p_\perp}} \Big[\sqrt{\frac{N-N_1}{N}} \sin\frac{\theta}{2} D(N-1, N_1) - \sqrt{\frac{N_1}{N}} e^{-i\phi} \cos\frac{\theta}{2} D(N-1, N_1-1) \Big], \tag{40}$$

with

$$p = \cos^2\frac{\theta}{2} - \frac{N_1}{N}\cos\theta, \tag{41}$$

$$p_\perp = \sin^2\frac{\theta}{2} + \frac{N_1}{N}\cos\theta. \tag{42}$$

Determination of the general form of negativity over a bipartition of states of the form $|D\rangle, |D_\perp\rangle$, and the subsequent analytical optimization is a difficult task. However, our numerical analysis suggests that the optimization of localizable negativity, in the current situation, always takes place in the σ^z basis. Using this information, $|D\rangle, |D_\perp\rangle$ and $p, p_\perp$ become

$$|D\rangle = |D(N-1, N_1)\rangle, \quad |D_\perp\rangle = |D(N-1, N_1-1)\rangle, \tag{43}$$

and

$$p = (N-N_1)/N; \; p_\perp = N_1/N, \tag{44}$$

respectively, resulting in

$$\langle E_{A_1A_2}\rangle = \max_{i,j,i\neq j} \frac{N-N_1}{N\binom{N-1}{N_1}} \sqrt{\binom{N-2}{N_1-i}\binom{N-2}{N_1-j}} + \max_{i,j,i\neq j} \frac{N_1}{N\binom{N-1}{N_1-1}} \sqrt{\binom{N-2}{N_1-1-i}\binom{N-2}{N_1-1-j}}. \tag{45}$$

It is easy to numerically check that $E_{A_1A_2:B} \geq \langle E_{A_1A_2}\rangle$, which approaches equality as N increases. Note also that the variation of $\langle E_{A_1A_2}\rangle$ with $E_{A_1A_2:B}$ is non-monotonic for lower values of N_1, resulting in a larger difference between $\langle E_{A_1A_2}\rangle$ and $E_{A_1A_2:B}$ at higher N. However, these features disappear as N_1 increases. See Fig. 3A.

a. Generalized Dicke states. Using the Dicke states, one can define an N-qubit permutation-symmetric state in the form of a *generalized* Dicke (gD) state [42], as

$$|D(N)\rangle = \sum_{N_1=0}^{N} a_{N_1} |D(N,N_1)\rangle , \tag{46}$$

where $a_{N_1} \in \mathbb{C}$, and $\sum_{N_1=0}^{N} |a_{N_1}|^2 = 1$. Due to a large number of state parameters, analytical calculation is difficult for gD states. However, as in the case of the Dicke states, the permutation symmetry can be used here also to have $E_{A_1:A_2B} = E_{A_1A_2:B}$ in the case of $n = m < N/2$ ($n = m < (N-1)/2$) for even (odd) N. This implies that it is sufficient to look into the relation between $\langle E_{A_1A_2}\rangle$ and $\min\{E_{A_1:A_2B}, E_{A_2:A_1B}\}$, which is given by (3). Moreover, our numerical results suggest that $\min\{E_{A_1:A_2B}, E_{A_2:A_1B}\} = E_{A_1:A_2B}$ for all Haar uniformly generated gD states, which leads to the upper bound of $\langle E_{A_1A_2}\rangle$ as $\langle E_{A_1A_2}\rangle \leq E_{A_1A_2:B}$ (see Fig. 3B). It is clear from the scatter diagrams that as N increases, the difference between $E_{A_1A_2:B}$ and $\langle E_{A_1A_2}\rangle$ decreases, and considerably larger fraction of states are found to obey $\langle E_{A_1A_2}\rangle = E_{A_1A_2:B}$ in the situation where each of the subsystems B and A_1 holds only one qubit.

D. Arbitrary multi-qubit pure states

In this section, we investigate the question posed in Sec. I for arbitrary states of systems with arbitrary number of qubits.

a. Three-qubit systems. While analytical calculation of the relevant quantities is difficult for large number of qubits, in relation to Proposition II, some analytical results can be derived for the three-qubit systems ($N = 3$) with $n = m = 1$. Note that the three-qubit gW states are a subset of the three-qubit W class states, which, together with the three-qubit GHZ class states, form the complete set of three-qubit pure states [61]. We explore whether the bound in Proposition II also applies to the three-qubit W class states given by [61]

$$|\psi_{\rm W}\rangle = a_0 |000\rangle + a_1 |100\rangle + a_2 |010\rangle + a_3 |001\rangle , \tag{47}$$

where $\sum_{i=0}^{3} |a_i|^2 = 1$ and $a_i \in \mathbb{C}$, $i = 0,1,2,3$. For ease of discussion, we consider the qubits 1, 2, and 3 to be subsystems B, A_1, and A_2, respectively. Also, we first consider the subclass of the W-class states with real coefficients only, i.e., $a_i \in \mathbb{R}$, $i = 0,1,2,3$, and numerically verify that the negativity over different bipartitions of the three-qubit W-class states are given by

$$E_{1:23} = 2\left|a_1\sqrt{a_2^2+a_3^2}\right| , \tag{48}$$

$$E_{2:13} = 2\left|a_2\sqrt{a_1^2+a_3^2}\right| , \tag{49}$$

$$E_{3:12} = 2\left|a_3\sqrt{a_1^2+a_2^2}\right| . \tag{50}$$

Further, performing local projection measurements in the basis $\{|b_0\rangle , |b_1\rangle\}$ on the qubit 1, one obtains the post-measured states on qubits 2 and 3 to be in the same form as in Eq. (22) with f_0^k and f_1^k ($k = 0,1$) given in Appendix B. Similar to the three-qubit gW states, negativity of the post-measured states are independent of the measurement-basis, and are given by $2|a_2||a_3|$. This leads to

$$\langle E_{23}\rangle = 2|a_2||a_3|. \tag{51}$$

We are now in a position to present the following proposition for the W class states of three qubits.

■ **Proposition IV.** *In the space $(E_{1:23}, \langle E_{23}\rangle)$, the localizable entanglement $\langle E_{23}\rangle$ of a 3-qubit normalized W-class state with real coefficients is upper bounded by the line*

$$\langle E_{23}\rangle = \frac{1}{2}\left(1+\sqrt{1-E_{1:23}^2}\right), \tag{52}$$

where $E_{1:23}$ is the bipartite entanglement over the bipartition $1:23$ in the state prior to measurement on the qubit 1.

Proof. Similar to the case of the gW states, we can write $\langle E_{23}\rangle^2$ as

$$\langle E_{23}\rangle^2 = 4a_2^2(1-a_0^2-a_1^2-a_2^2). \tag{53}$$

For a fixed value of $a_0^2+a_1^2 = a^2$, the maximum of $\langle E_{23}\rangle^2$, and therefore of $\langle E_{23}\rangle$ occurs at $a_2^2 = (1-a^2)/2$, the maximum value of $\langle E_{23}\rangle$ being $(1-a^2)$. Also, $E_{1:23} = 2\left|a_1\sqrt{1-a^2}\right|$. Note that the maximum value of $\langle E_{23}\rangle$ as well as $E_{1:23}$ have two free parameters, a_0 and a_1, constrained by $a_0^2+a_1^2$ being a constant, a^2. Eliminating a_1 from $\langle E_{23}\rangle$ and $E_{1:23}$, followed by solving for $\langle E_{23}\rangle$ leads to

$$\langle E_{23}\rangle = \frac{1}{2}\left[(1-a_0^2)+\sqrt{(1-a_0^2)^2-E_{1:23}^2}\right], \tag{54}$$

where $0 \leq a_0^2 \leq a^2$. Further maximization w.r.t. a_0 implies $a_0 = 0$, leading to Eq. (52). □

Similar to the three-qubit gW states, the following Corollaries originate from Proposition IV.

◇ **Corollary IV.1.** *The family of W class states with real coefficients that satisfy Eq. (52) are given by*

$$a_2^2 = a_3^2 = (1-a_1^2)/2. \tag{55}$$

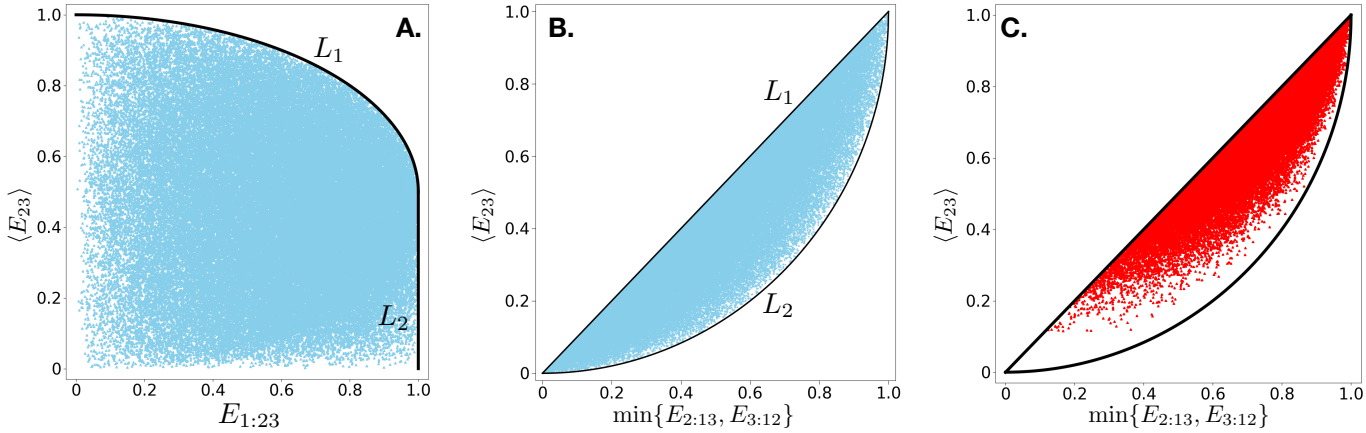


FIG. 4. **W-class states.** Scatter plot of a sample of 10^7 Haar-uniformly generated three-qubit W-class states on the **A.** $(E_{1:23}, \langle E_{23}\rangle)$ and the **B.** $(\min\{E_{2:13}, E_{3:12}\}, \langle E_{23}\rangle)$ plane. The lines $L1$ and $L2$ bounding the states correspond to Eq. (52) and $E_{1:23} = 1$ respectively. **C.** A sample of 10^7 Haar-uniformly generated GHZ-class states are also found to be bound by the same upper and lower bounds as proposed in Proposition III. Both the axes of all the figure are dimensionless.

Proof. The proof of this Corollary follows from the maximization condition of $\langle E_{23}\rangle$, and the normalization of the W-class state. □

◇ **Corollary IV.2.** *For the family of W-class states given by Eq. (55),* $E_{2:13} = E_{3:12}$.

Proof. The proof of this corollary follows from identifying the states satisfying Eq. (55) as the three-qubit gW states, and from the proof of Corollary II.2. □

■ **Proposition V.** *In* $(\min\{E_{2:13}, E_{3:12}\}, \langle E_{23}\rangle)$ *space, the localizable entanglement* $\langle E_{23}\rangle$ *of a three-qubit normalized W-class state with real coefficients is upper-bounded by the line*

$$\langle E_{23}\rangle = \min\{E_{2:13}, E_{3:12}\}, \tag{56}$$

and lower-bounded by the line

$$\langle E_{23}\rangle^2 - 2\langle E_{23}\rangle + (\min\{E_{2:13}, E_{3:12}\})^2 = 0, \tag{57}$$

where $E_{2:13}$ $(E_{3:12})$ *is the bipartite entanglement over the bipartition* $2:13$ $(3:12)$ *in the state prior to measurement on the qubit* 1.

Proof. Similar to the proof of Proposition III, the upper bound follows from the monotonicity of E (see Eq. (3)). To prove the lower bound, we start by assuming $E_{2:13} \geq E_{3:12}$ and $\min\{E_{2:13}, E_{3:12}\} = E_{3:12}$, which, by virtue of Eqs. (49) and (50), implies $a_2^2 \geq a_3^2$. For a fixed a_3 and a_0, $\langle E_{23}\rangle$ is minimum if a_2 is minimum, leading to $a_2 = a_3$, and subsequently $\langle E_{23}\rangle \geq 2a_3^2$. On the other hand, exploiting normalization of the W-class state, $E_{3:12} = 2\left|a_3\sqrt{1-a_0^2-a_3^2}\right|$. Eliminating a_3 from $E_{3:12}$ and the minimum of $\langle E_{23}\rangle$, we obtain

$$\langle E_{23}\rangle^2 + E_{3:12}^2 - 2\langle E_{23}\rangle(1-a_0^2) = 0. \tag{58}$$

Similar to Proposition V, it can be shown that $\langle E_{23}\rangle$ attains a minimum for $a_0 = 0$, leading to Eq. (57). □

Note 3. Similar to the case of N-qubit gW states, in this case also, we numerically verify that the Propositions IV and V remain valid in the case of generic three-qubit states from W class with complex coefficients. The bounds in the case of three-qubit W class states are demonstrated in Fig. 4A-B.

Note 4. We also investigate the three-qubit GHZ class states, given by

$$|\psi_{\text{GHZ}}\rangle = \sum_{i=0}^{7} c_i\,|\phi_i\rangle\,, \tag{59}$$

with $c_i \in \mathbb{C}$ and $\{|\phi_i\rangle\,; i = 0, 1, \cdots, 7\}$ being the standard product basis in the Hilbert space of three qubits. While analytical investigation is difficult due to a large number of parameters involved in these states, our numerical analysis does not provide any evidence of the existence of an upper bound of $\langle E_{23}\rangle$ on the $(E_{1:23}, \langle E_{23}\rangle)$ plane. However, our investigation involving a sample of 10^7 Haar-uniformly generated GHZ-class states did not find any example that violates the lower bound proposed in Proposition V (see Fig. 4C for a demonstration). While this does not analytically prove the validity of the lower bound, this implies that Proposition IV *has the potential to distinguish between the three-qubit W class states from the GHZ class states*.

b. Larger systems. In order to study the correlation between localizable entanglement $\langle E_{A_1A_2}\rangle$ and the bipartite entanglement lost due to the measurement, namely, $E_{A_1A_2:B}$, $E_{A_1:A_2B}$, and $E_{A_2:A_1B}$ in the case of pure states on N-qubits, we look into how the states are distributed on the $(E_{A_1A_2:B}, \langle E_{A_1A_2}\rangle)$ and the $(\min[E_{A_1:A_2B}, E_{A_2:A_1B}], \langle E_{A_1A_2}\rangle)$ spaces. To investigate this, we define the followings.

$$\delta_1 = \langle E_{A_1A_2}\rangle - E_{AB}, \tag{60}$$
$$\delta_2 = \langle E_{A_1A_2}\rangle - \min\{E_{A_1B:A_2}, E_{A_2B:A_1}\}. \tag{61}$$

Note that $\delta_1 \geq 0$ $(\delta_2 \geq 0)$ implies $\langle E_{A_1A_2}\rangle \geq E_{A_1A_2:B}$ $(E_{A_1A_2}\rangle \geq \min\{E_{A_1B:A_2}, E_{A_2B:A_1}\})$, which is representative of a situation where one can, on average, localize at least

$E_{A_1A_2:B}$ ($\min\{E_{A_2:A_1B}, E_{A_1:A_2B}\}$) amount of entanglement via local projection measurements on the qubits in B. The percentages of N-qubit states for which $\delta_1 > 0$ are included in Table I for different combinations of N and m, keeping $n = 1$, where in each case, a sample of 10^5 Haar-uniformly generated pure states are considered. Clearly, the percentage of states for which $\delta_1 > 0$ increases overall with the increase in the number of qubits, implying that the number of states for which $\langle E_{A_1A_2}\rangle > E_{A_1A_2:B}$ are more for larger systems. However, the percentage of states for which $\delta_1 = 0$, up to our numerical accuracy, is negligibly small for all cases of (N, n, m). On the other hand, as expected, $\delta_2 > 0$ does not occur for any multi-qubit pure states, as it would imply a violation of (3). Moreover, for a very small fraction of states, $\delta_2 = 0$. This fraction overall increases with an increase in the number of qubits in the system.

III. QUANTUM STATES UNDER PHASE-FLIP NOISE

It is now logical to ask whether and how the results reported in Sec. II are modified if the multi-qubit system is subjected to noise [67]. In this paper, we consider a situation where qubits of the multi-qubit system are sent through independent phase-flip channels [67, 68]. These phase-flip channels can be either Markovian [69], or non-Markovian [70–72]. Using the Kraus operator representation, the evolution of the quantum state $\rho_0 = |\psi\rangle\langle\psi|$ under these phase-flip channels are given by

$$\rho = \sum_\alpha K_\alpha \rho_0 K_\alpha^\dagger, \tag{62}$$

such that $\sum_\alpha K_\alpha^\dagger K_\alpha = I$, I being the identity operator in the Hilbert space of the multi-qubit system, and Kraus operators $\{K_\alpha\}$, takes the form $K_\alpha = \sqrt{p_\alpha} K'_\alpha$ with

$$K'_\alpha = \bigotimes_{i=1}^{N} K'_{\alpha_i};\ p_\alpha = \prod_{i=1}^{N} p_{\alpha_i}. \tag{63}$$

Here, the index $\alpha \equiv \alpha_1\alpha_2\cdots\alpha_N$ is interpreted as a multi-index, $\sum_{\alpha_i} p_{\alpha_i} = 1$, and K'_{α_i} are the single-qubit Kraus operators, the form of which depends on the type of noise under consideration. In the case of the phase-flip noise, $\alpha_i \in \{0, 1\}$, $K'_{\alpha_i=0} = I_i$, and $K'_{\alpha_i=1} = \sigma_i^z$, with

$$p_{\alpha_i=0} = 1 - \frac{q}{2},\ p_{\alpha_i=1} = \frac{q}{2} \tag{64}$$

in the Markovian case [69], and

$$\begin{aligned} p_{\alpha_i=0} &= \left(1 - \frac{q}{2}\right)\left(1 - \frac{\alpha q}{2}\right), \\ p_{\alpha_i=0} &= \left[1 + \alpha\left(1 - \frac{q}{2}\right)\right]\frac{q}{2} \end{aligned} \tag{65}$$

in the non-Markovian case [70–72]. Here, q is the *noise strength* ($0 \le q \le 1$), and α is the non-Markovianity parameter ($0 \le \alpha \le 1$). For ease of discussion, from now onward, we denote entanglement in the noiseless scenario with a superscript "0". For example, $\langle E_{A_1A_2}\rangle^0$ and E^0_{AB} denote the localizable entanglement over the subsystem A and the bipartite entanglement over the bipartition $A : B$ of the system in the case of ρ_0.

A. Generalized GHZ states

We start our discussions with the N-qubit gGHZ state subjected to phase-flip noise on all qubits. In this situation, we prove the following proposition.

■ **Proposition VI.** *For any tripartition $A_1 : A_2 : B$ of an N-qubit gGHZ state under uncorrelated phase-flip channel on all qubits,*

$$\langle E_{A_1A_2}\rangle = E_{A_1A_2:B} = E_{A_1:A_2B} = E_{A_2:A_1B}, \tag{66}$$

irrespective of whether the noise is Markovian, or non-Markovian.

Proof. The N-qubit gGHZ state, under the Markovian phase-flip noise on all qubits, takes the form

$$\begin{aligned} \rho = &\left(|a_0|^2(|0\rangle\langle 0|)^{\otimes N} + |a_1|^2(|1\rangle\langle 1|)^{\otimes N}\right) \\ &+(1-q)^N\left(a_0a_1^*(|0\rangle\langle 1|)^{\otimes N} + a_0^*a_1(|1\rangle\langle 0|)^{\otimes N}\right) \end{aligned} \tag{67}$$

Partial transposition of ρ with respect to the subsystems B leads to

$$\begin{aligned} \rho^{T_B} = &\left(|a_0|^2(|0\rangle\langle 0|)^{\otimes N} + |a_1|^2(|1\rangle\langle 1|)^{\otimes N}\right) \\ &+(1-q)^N a_0a_1^*(|0\rangle\langle 1|)^{\otimes N-n}(|1\rangle\langle 0|)^{\otimes n} \\ &+(1-q)^N a_0^*a_1(|1\rangle\langle 0|)^{\otimes N-n}(|0\rangle\langle 1|)^{\otimes n}, \end{aligned} \tag{68}$$

with non-zero eigenvalues $|a_0|^2, |a_1|^2, \pm(1-q)^N|a_0||a_1|$. Therefore the entanglement between partition A and partition B, as quantified by negativity [56–60], is given by

$$\begin{aligned} E_{A_1A_2:B} &= 2(1-q)^N|a_0|\sqrt{1-|a_0|^2} \\ &= (1-q)^N E^0_{A_1A_2:B}. \end{aligned} \tag{69}$$

To calculate the localizable entanglement over the subsystem A with bipartition $A_1 : A_2$, we proceed as in the case of Proposition I, and write the post-measured states on A as

$$\tilde{\rho}_A^k = \mathrm{Tr}_B\left[\left(M^k\rho M^{k\dagger}\right)/p_k\right], \tag{70}$$

which, written explicitly, takes the form

$$\begin{aligned} \tilde{\rho}_A^k = \frac{1}{p_k}\Big[&\Big\{|a_0|^2|f_0^k|^2(|0\rangle\langle 0|)^{\otimes N-n} \\ &+|a_1|^2|f_1^k|^2(|1\rangle\langle 1|)^{\otimes N-n}\Big\} \\ &+(1-q)^N\big\{a_0a_1^*f_0^kf_1^{k*}(|0\rangle\langle 1|)^{\otimes N-n} \\ &+a_0^*a_1f_1^kf_0^{k*}(|1\rangle\langle 0|)^{\otimes N-n}\big)\big\}\Big], \end{aligned} \tag{71}$$

with

$$p_k = \left(|a_0|^2|f_0^k|^2 + |a_1|^2|f_1^k|^2\right). \tag{72}$$

Partial transposition of $\tilde{\rho}_A^k$ over any bipartition $A_1 : A_2$, and subsequent calculation of negativity followed by the optimization of average negativity over $A_1 : A_2$ yields

$$\langle E_{A_1:A_2}\rangle = 2(1-q)^N|a_0|\sqrt{1-|a_0|^2}\left[\max\sum_{k=0}^{2^n-1}|f_0^k||f_1^k|\right], \tag{73}$$

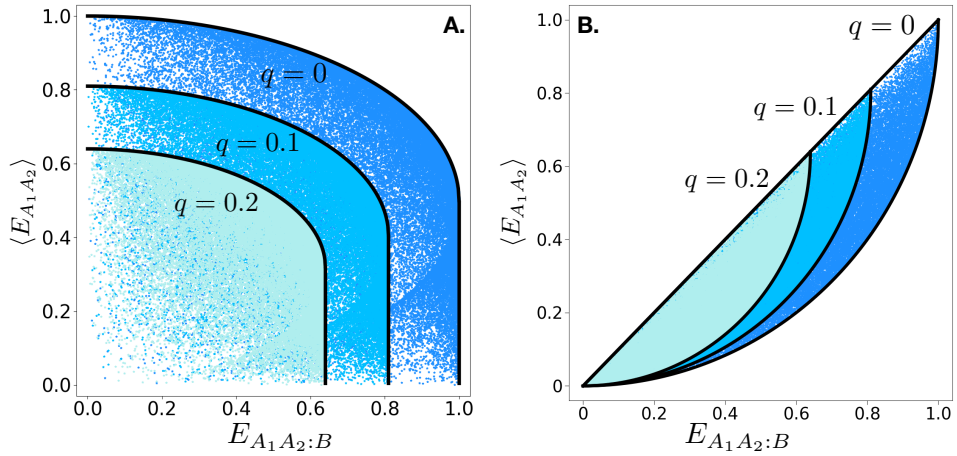


FIG. 5. **Generalized W states under Markovian phase-flip channels.** Modification of boundaries of gW states proposed in Propositions II and III on the **A.** $(E_{A_1A_2:B}, \langle E_{A_1A_2} \rangle)$ and the **B.** $(\min\{E_{A_1:A_2B}, E_{A_2:A_1B}\}, \langle E_{A_1A_2} \rangle)$ plane due to Markovian phase-flip noise of noise strength $q = 0, 0.1, 0.2$ (see also Fig. 2). The modified boundaries are given in Propositions VI and VII. Note that the trivial boundaries corresponding to zero entanglement lines are not shown. All the axes on all figures are dimensionless.

as in Eq. (14). The maximization is similar to that shown in the proof of Proposition I, leading to

$$\langle E_{A_1:A_2} \rangle = (1-q)^N \langle E_{A_1A_2} \rangle^0 = E_{A_1A_2:B}. \tag{74}$$

Also, from the symmetry of ρ, $E_{A_1A_2:B} = E_{A_1:A_2B} = E_{A_2:A_1B}$, leading to Eq. (66).

Same line of calculations would follow for the non-Markovian phase-flip channel, leading to

$$\begin{aligned} E_{A_1A_2:B} &= |1 - f(q,\alpha)|^N \, E^0_{A_1A_2:B}, \\ \langle E_{A_1A_2} \rangle &= |1 - f(q,\alpha)|^N \, \langle E_{A_1A_2} \rangle^0, \end{aligned} \tag{75}$$

with

$$f(q,\alpha) = q\left\{1 + \alpha\left(1 - \frac{q}{2}\right)\right\}, \tag{76}$$

which implies $\langle E_{A_1A_2} \rangle = E_{A_1A_2:B}$. Similar proof follows for $E_{A_1:A_2B}$, and $E_{A_2:A_1B}$ also, resulting in Eq. (66) for the non-Markovian phase-flip channel. Hence the proof. □

Note 5. A comparative discussion on the variation of entanglement with q in the cases of the Markovian and the non-Markovian phase-flip channels is in order here. Note that in the former case, entanglement decays monotonically with q, as indicated from the $(1-q)^N$ dependence, while the decay fastens exponentially with increasing number of qubits. It also indicates that entanglement vanishes asymptotically with increasing q, attaining zero value only at $q = 1$. Similar features are also present in the case of the non-Markovian channel, except one where in contrast to entanglement vanishing only at $q = 1$ in the former case, entanglement vanishes at a finite critical q in the latter, given by

$$q_c = \frac{1}{\alpha}\left(1 + \alpha - \sqrt{1+\alpha^2}\right). \tag{77}$$

For $q > q_c$, entanglement revives again. Note that q_c is a monotonically decreasing function of α, which, in the limit $\alpha \to 0$ (the Markovian limit), goes to 1.

B. Generalized W states

We now focus on the N-qubit gW states under the phase-flip noise on all qubits. Analytical investigation of $\langle E_{A_1A_2} \rangle$ as well as bipartite entanglement over the unmeasured state in such cases is difficult due to the increasing number of state as well as optimization parameters. However, our numerical investigation suggests that irrespective of the tripartition $A_1 : A_2 : B$ of the N-qubit system, the optimization of $\langle E_{A_1A_2} \rangle$ always takes place via σ^z measurement on all qubits $i \in B$. This result can be utilized to determine the dependence of $\langle E_{A_1A_2} \rangle$ and $E_{A_1A_2:B}$ on the noise strength q, and extend the Propositions II and III, as follows.

a. Markovian phase-flip channels. In the case of the Markovian phase-flip channels, we obtain[3]

$$\langle E_{A_1A_2} \rangle = (1-q)^2 \langle E_{A_1A_2} \rangle^0, \tag{78}$$

$$E_{A_1A_2:B} = (1-q)^2 E^0_{A_1A_2:B}, \tag{79}$$

Given these results, we present the following Proposition.

■ **Proposition VII.** *In the space $(E_{A_1A_2:B}, \langle E_{A_1A_2} \rangle)$, the localizable entanglement $\langle E_{A_1A_2} \rangle$ of an N-qubit normalized gW state subjected to Markovian phase-flip channels of the same strength, q, on all qubits is bounded by the lines*

$$\langle E_{A_1A_2} \rangle = \frac{1}{2}\left[(1-q)^2 + \sqrt{(1-q)^4 - E^2_{A_1A_2:B}}\right], \tag{80}$$

and

$$E_{A_1A_2:B} = (1-q)^2, \tag{81}$$

where $E_{A_1A_2:B}$ is the bipartite entanglement over the bipartition $A_1A_2 : B$ in the state prior to measurement on all the qubits in B.

[3] These expressions are determined for systems of small sizes, and are verified numerically for larger systems with different combinations of (N, n, m).

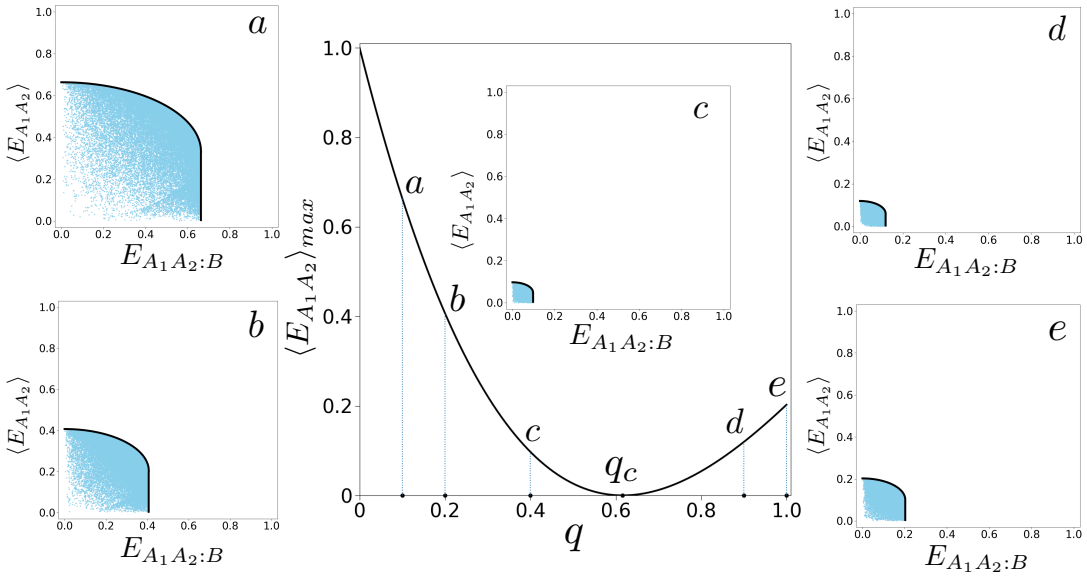


FIG. 6. **Generalized W states under non-Markovian phase-flip noise.** The variation of $\langle E_{A_1A_2}\rangle$ as a function of q (Eq. (84)), with $\langle E_{A_1A_2}\rangle^0 = 1$ and $\alpha = 0.9$, exhibiting monotonic decay followed by a vanishing at q_c (Eq. (77)), and a subsequent revival for $q > q_c$. In the entire range $0 \leq q \leq 1$, five values of noise strengths, namely a. $q = 0.1$, b. $q = 0.2$, c. $q = 0.4$, d. $q = 0.9$, and e. $q = 1.0$ are chosen, and the modification of the boundaries on the gW states, as given in Proposition II, with varying q is demonstrated. The region accessible by the gW states on the $(E_{A_1A_2:B}, \langle E_{A_1A_2}\rangle)$ decreases at first, vanishes at $q = q_c$, and then revives again. The axes on all figures are dimensionless.

Note 6. It is worthwhile to note that the line given in Eq. (81) corresponds to the family of states, described by Eq. (36), subjected to the single-qubit phase-flip channels on all qubits.

Note 7. Proposition VI implies that the area on the $(E_{A_1A_2:B}, \langle E_{A_1A_2}\rangle)$ plane confining the noisy gW states shrinks with increasing noise strength q, and vanishes at $q = 1$. This is demonstrated in fig. 4A.

Noting that $E_{A_1:A_2B}$ and $E_{A_2:A_1B}$ also have similar dependence on q as $E_{A_1A_2:B}$, Proposition III can be extended to the case of gW states under phase-flip noise, as follows.

■ **Proposition VIII.** *In* $(\min\{E_{A_1:A_2B}, E_{A_2:A_1B}\}, \langle E_{A_1A_2}\rangle)$ *space, the localizable entanglement* $\langle E_{A_1A_2}\rangle$ *of an* N*-qubit normalized gW state subjected to the phase-flip channel of strength* q *on all qubits is upper-bounded by the line*

$$\langle E_{A_1A_2}\rangle = \min\{E_{A_1:A_2B}, E_{A_2:A_1B}\}, \tag{82}$$

and lower-bounded by the line

$$\langle E_{A_1A_2}\rangle^2 - 2(1-q)^2\langle E_{A_1A_2}\rangle + \left(\min\{E_{A_1:A_2B}, E_{A_2:A_1B}\}\right)^2 = 0, \tag{83}$$

where $E_{A_1:A_2B}$ $(E_{A_2:A_1B})$ *is the entanglement over the bipartition* $A_1 : A_2B$ $(A_2 : A_1B)$ *in the state prior to measurement on all the qubits in* B.

b. Non-Markovian phase-flip channels. A similar approach can also be taken in the case of the non-Markovian channels, where entanglement has the following dependence on q and α:

$$\langle E_{A_1A_2}\rangle = |1 - f(q,\alpha)|^2 \langle E_{A_1A_2}\rangle^0, \tag{84}$$

$$E_{A_1A_2:B} = |1 - f(q,\alpha)|^2 E^0_{A_1A_2:B}, \tag{85}$$

$$E_{A_1:A_2B} = |1 - f(q,\alpha)|^2 E^0_{A_1:A_2B}, \tag{86}$$

$$E_{A_2:A_1B} = |1 - f(q,\alpha)|^2 E^0_{A_2:A_1B}, \tag{87}$$

with $f(q,\alpha)$ given in Eq. (76). Using these, one can straightforwardly obtain the results on the bounds on the gW states when subjected to non-Markovian phase-flip channels, by replacing the $(1-q)^2$ factors with $|1 - f(q,\alpha)|^2$. To keep the text uncluttered, we refrain from writing these Propositions explicitly.

Similar to the Markovian case, for a fixed value of α, the area on the $E_{A_1A_2:B} - \langle E_{A_1A_2}\rangle$ plane confining the noisy gW states shrinks with increasing q in the case of the non-Markovian phase flip channel also. However, in contrast to the Markovian case, the area vanishes at a critical noise strength q_c, given in Eq. (77), and then revives again for $q > q_c$ (see Fig. 4B for a demonstration). It is worthwhile to note that the decay of entanglement in the case of the gW states under Markovian and non-Markovian phase-flip channel is independent of the number of qubits in the system, as opposed to the case of the gGHZ states, where the dependence is exponential in N.

C. Numerical results

The complexity of the states obtained via applying single-qubit phase-flip noise to all qubits of a multi-qubit states prevents analytical investigation into the relation between the localizable end the destroyed entanglement in most of the cases. In this subsection, we discuss the numerical results obtained for the mixed states generated via subjecting three-qubit W-class states, N-qubit Dicke and gD states, and arbitrary N-qubit pure states to Markovian and non-Markovian phase-flip channels.

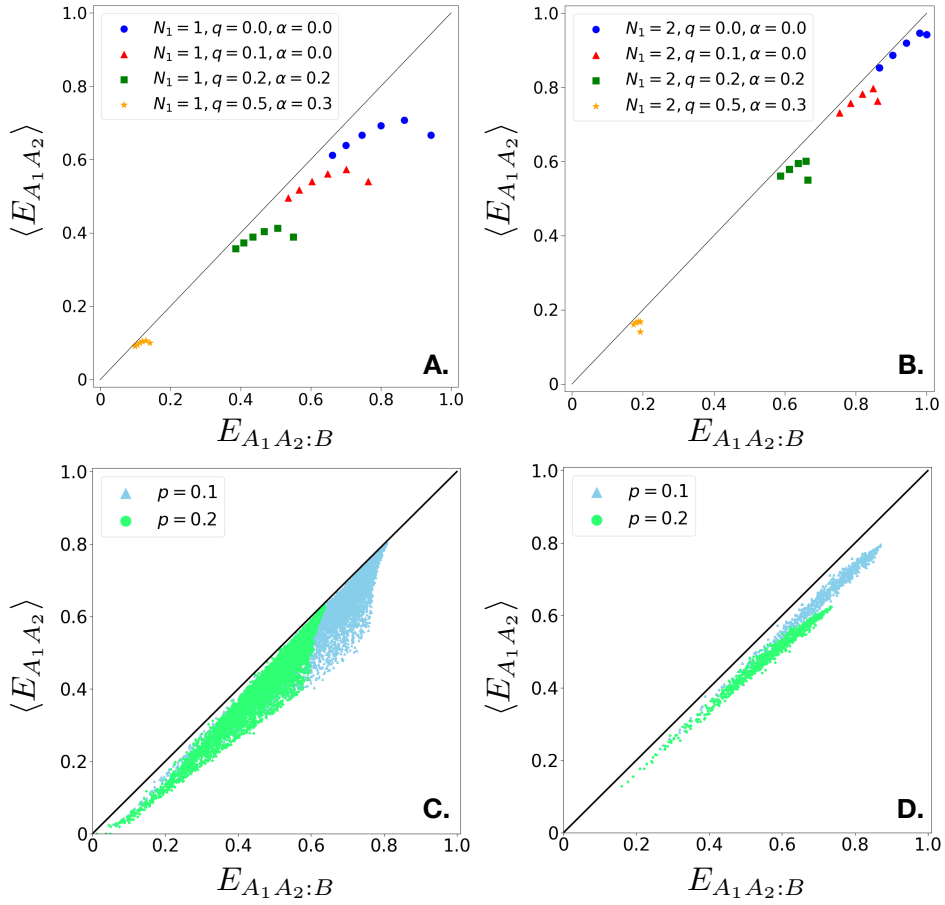


FIG. 7. **Dicke and generalized Dicke states under phase-flip noise. A., B.** Scatter plots of N-qubit Dicke states, for upto $N = 8$, under Markovian and non-Markovian phase-flip noise are shown on the $(E_{A_1A_2:B}, \langle E_{A_1A_2} \rangle)$ planes for **A.** $N_1 = 1$, and **B.** $N_1 = 2$. **C., D.** On the other hand, scatter plots of samples of 10^7 gD states with **C.** $N = 3$ and **D.** $N = 4$ are shown on the $(E_{A_1A_2:B}, \langle E_{A_1A_2} \rangle)$ plane. All axes in all of the figures are dimensionless.

a. Three-qubit states. Our numerical investigation of the three-qubit W-class states subjected to Markovian as well as non-Markovian phase-flip channels indicate that the variations of the localizable entanglement $\langle E_{23} \rangle$ as well as the bipartite entanglement lost during measurement, namely, $E_{1:23}$, $E_{2:13}$, and $E_{3:12}$, are identical to that described in Eqs. (78)-(79) (Markovian) and Eqs. (84)-(87) (non-Markovian). This implies that the mixed states obtained from the three-qubit W-class states, for a specific noise strength q, are bounded in a similar way as described for the gW states under phase-flip noise. On the other hand, while a similar numerical analysis is difficult for the GHZ class states due to the increased number of parameters, we observe that similar to the pure GHZ-class states discussed in Note 4 (see also Fig. 4C.), the bounds proposed in Eqs. (82)-(83) hold also for three-qubit GHZ-class states subjected to the Markovian phase-flip noise channels.

b. Dicke states and generalized Dicke states under noise. We also numerically investigate the N-qubit Dicke and gD states subjected to Markovian and non-Markovian phase-flip channels. Fig. 7A-B depict the scatter plots of the Dicke states up to $N = 8$, and $N_1 = 1, 2$, where Markovian and non-Markovian phase-flip channel is applied to all qubits. It is clear from the figures that similar to the case of the Pure Dicke states (see Sec. II D), (a) the variation of $\langle E_{A_1A_2} \rangle$ with $E_{A_1A_2:B}$ remains non-monotonic, and (b) with increasing N_1, the states

N	n	m	Fraction of states (in %) with $\delta_1 > 0$				
			$q = 0.0$	$q = 0.1$	$q = 0.2$	$q = 0.3$	$q = 0.4$
3	1	1	23.343%	23.608%	23.097%	21.530%	18.890%
4	1	1	38.704%	20.461%	15.757%	15.514%	15.336%
5	1	1	44.920%	14.213%	12.942%	10.531%	07.487%
5	1	2	100.00%	100.00%	100.00%	100.00%	93.402%

TABLE I. Variations of the fraction of Haar uniformly generated three-, four-, and five-qubit states for which $\delta_1 > 0$, as a function of the noise parameter q, which assumes five values, $q = 0.0, 0.1, 0.2, 0.3$, and 0.4, from left to right along the row for a specific combination of N, n, and m, in the case of the Markovian phase-flip noise. In all cases, we have kept $n = 1$, where n and m being the sizes of B and A_1 respectively. For the three-qubit system, only GHZ class states are considered. For each case, the percentages are determined from a sample size of 10^5 Haar-uniformly generated states. All the quantities presented in the table are dimensionless.

tend to the $\langle E_{A_1A_2}\rangle = E_{A_1A_2:B}$ line. Also, increasing the non-Markovianity factor α generally tends to lower values of $\langle E_{A_1A_2}\rangle$ and $E_{A_1A_2:B}$.

In the case of the gD states, our numerical investigation suggests that while the upper bound $\langle E_{A_1A_2}\rangle \leq E_{A_1A_2:B}$ remains valid even in the presence of phase-flip noise irrespective of whether it is Markovian, or non-Markovian. However, with increasing number of qubits, as in the case of the pure gD states, more states are concentrated close to the $\langle E_{A_1A_2}\rangle = E_{A_1A_2:B}$ line, although the number of states for which $\langle E_{A_1A_2}\rangle = E_{A_1A_2:B}$ diminishes drastically. This is demonstrated in Fig. 7C-D for gD states with $N = 3, 4$ qubits, respectively, under Markovian phase-flip noise. The results remain qualitatively the same even in the presence of non-Markovian phase-flip noise also.

c. Arbitrary pure states under noise. It is important to note that the numerical investigation for arbitrary N-qubit pure states subjected to phase-flip channels is resource-intensive even for a small number of qubits due to the optimization involved in the computation of localizable entanglement, as the number of optimization parameter increases with increasing n, the size of the measured subsystem B. In this paper, we restrict ourselves in reporting data for which B is constituted of one qubit only. Similar to the pure states of N-qubits described in Sec. II D, we focus on δ_1 and δ_2 (Eqs. (60)-(61)) also for the mixed states obtained by subjecting N-qubit arbitrary pure states to Markovian phase-flip channels. As expected, for all investigated values of q, no states are found for which $\delta_2 \geq 0$, implying a violation of inequality (3), which is similar to the case of the pure states (see Sec. II D). On the other hand, the percentage of states for which $\delta_1 > 0$ are tabulated in Table I for different noise strengths in the case of the Markovian phase-flip channel. It is clear from the table that (a) for a fixed N with $n = 1$, the number of states for which $\delta_1 > 0$ overall decreases with increasing q, and (b) for a specific q value > 0, such states overall decreases in number with increasing N, as long as n and m are fixed at 1.

IV. INTERACTING 1D QUANTUM SPIN MODELS

It is natural to ask whether the bounds discussed in Sec. II for the pure states also exist in the ground states of paradigmatic quantum spin Hamiltonians. In order to investigate this, we focus on the one-dimensional (1D) quantum spin chains with N spin-1/2 particles, governed by a Hamiltonian given by [84]

$$H = \sum_{i=1}^{N}\Big[J^{xy}_{i,i+1}\Big\{(1+\gamma)\sigma^x_i\sigma^x_{i+1} + (1-\gamma)\sigma^y_i\sigma^y_{i+1}\Big\} + J^{zz}_{i,i+1}\sigma^z_i\sigma^z_{i+1} + h_i\sigma^z_i\Big]. \quad (88)$$

In Eq. (88), γ is the xy anisotropy parameter, h_i is local magnetic field strength corresponding to spin i, and $J^{xy}_{i,i+1}$ $\left(J^{zz}_{i,i+1}\right)$ represents the nearest-neighbor xy (zz) interaction strengths. Also, we assume periodic boundary condition (PBC) in the system, implying $\sigma^{x,y,z}_{N+1} \equiv \sigma^{x,y,z}_1$. A number of paradigmatic 1D quantum spin models can be represented by different special cases of H. In this paper we are interested in two of them, namely, (a) transverse-field XY model (TXY) $\left(0 < \gamma \leq 1, J^{zz}_{i,i+1} = 0\right)$ [74–79] (note that the transverse-field Ising model (TIM) [78, 79, 91] is a special case of the TXY model with $\gamma = 1$), and (b) XXZ model with magnetic field (XXZ) $(\gamma = 0)$ [80–85].

A. Ordered quantum spin models

In the case of the *ordered* quantum spin models where order exists in all spin-spin couplings as well as the field strengths, we assume $J^{xy}_{i,i+1} = J^{xy} > 0$, $J^{zz}_{i,i+1} = J^{zz} > 0$, and $h_i = h > 0$ for all $i = 1, 2, \cdots, N$. In such models, we numerically investigate the correlation between $\langle E_{A_1A_2}\rangle$ and $\{E_{A_1A_2:B}, E_{A_1B:A_2}, E_{A_2B:A_1}\}$ in the ground state, which is obtained via numerical diagonalization of H. We first consider the ordered AFM TXY model, and define $g = h/J^{xy}$ as the dimensionless field-strength. The model exhibits a quantum phase transition from an antiferromagnetic (AFM) phase $(g < 1)$ to a paramagnetic (PM) phase $(g > 1)$ at $g_c = 1$, for all values of $\gamma > 0$ [31, 75–79, 92, 93]. Fig. 8A. depicts the scatter plot of $\langle E_{A_1A_2}\rangle - E_{AB}$ corresponding to the ordered TXY model for different values of N, where for each N, values of $n, m = 1$. This, along with the PBC ensures that $E_{A_1A_2:B} = E_{A_1:A_2B}$, while our numerical findings suggest that for the ground states of these quantum spin models with $n = m = 1$, $\min\{E_{A_1:A_2B}, E_{A_2:A_1B}\}$ for all values of N. This implies that it is sufficient to investigate the dependence of $\langle E_{A_1A_2}\rangle$ on $E_{A_1A_2:B}$, which is demonstrated in Fig. 8A. In order to generate the scatter plot on the $E_{A_1A_2:B} - \langle E_{A_1A_2}\rangle$ plane, the values of g are chosen to be deep inside the AFM $(0.2 \leq g \leq 0.8)$ and the PM $(1.2 \leq g \leq 1.8)$ phases. It is evident from the figure that $\langle E_{A_1A_2}\rangle$ is positively correlated with E_{AB}. Irrespective of the value of N, the data suggests a quadratic dependence of $\langle E_{A_1A_2}\rangle$ on $E_{A_1A_2:B}$, given by

$$\langle E_{A_1A_2}\rangle = \lambda_2 E^2_{A_1A_2:B} + \lambda_1 E_{A_1A_2:B} + \lambda_0, \quad (89)$$

where the values of $\lambda_{0,1,2}$ can be obtained by fitting the numerical data to Eq. (89). In the present case, $\lambda_0 = -0.05 \pm 0.001$, $\lambda_1 = 1.09 \pm 0.008$, and $\lambda_2 = -0.05 \pm 0.007$. Our numerical investigation suggests that the form of Eq. (89) remains invariant with a change in the values of the xy anisotropy parameter γ.

In the case of the XXZ model in a magnetic field along the z direction with PBC, we assume $J^{zz} = \Delta J^{xy}$, where Δ signifies the z-anisotropy parameter, and denote the dimensionless field-strength by $g = h/J^{xy}$. For $-1 \leq \Delta \leq 1$, the model undergoes a quantum phase transition from the XY phase to the ferromagnetic (FM) phase at the critical field strength $g_c = \pm(1 + \Delta)$ [84]. Similar to the TXY model, we fix Δ and investigate the correlation between $\langle E_{A_1A_2}\rangle$ and E_{AB} deep inside the XY and the FM phases. The data is presented in Fig. 8B., which indicates qualitatively similar result as in the case of the TXY model. The fitted curve also has the form given in Eq. (89), with $\lambda_0 = -0.36 \pm 0.045$, $\lambda_1 = 1.92 \pm 0.106$, and $\lambda_2 = -0.70 \pm 0.061$. It is worthwhile to note that in the case of the XXZ model also, the overall re-

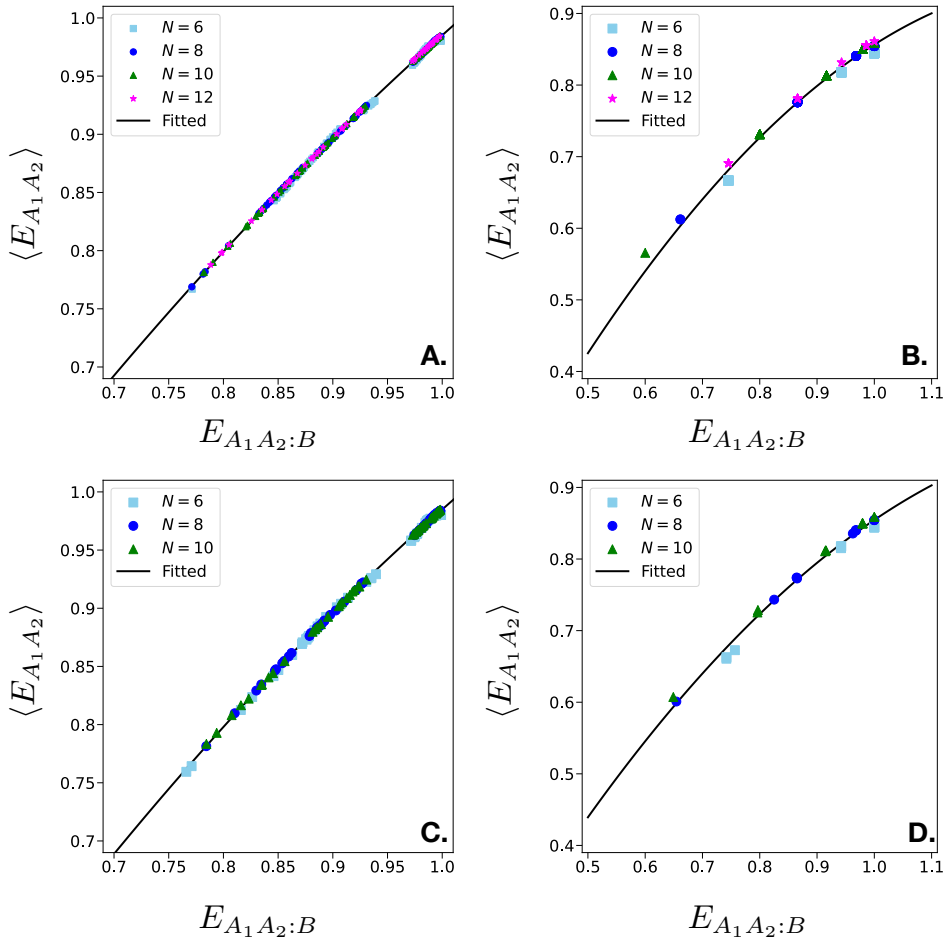


FIG. 8. **1D quantum spin models.** Scatter plot of the ground states in 1D TXY model (**A**,**C**), and 1D XXZ model in an external field (**B**,**D**) on the $(E_{A_1A_2:B}, \langle E_{A_1A_2} \rangle)$ plane for different values of N. The ordered cases are presented in **A** and **B**, while the disordered cases are depicted in **C** and **D**. The variations of $\langle E_{A_1A_2} \rangle$ as a function of $E_{A_1A_2:B}$ are fitted to Eq. (89). In the case of the TXY model, γ is taken to be 0.5 for both ordered and disordered cases, while for the XXZ model, $\Delta = 0.5$. In the disordered case, for both models, $\sigma_g = 0.05$. All axes in all figures are dimensionless.

lation between $\langle E_{A_1A_2} \rangle$ and $E_{A_1A_2:B}$ remains unaltered with a change in the value of Δ.

B. Disordered quantum spin models

In a *disordered* quantum spin model [73], the values of a relevant system parameter, such as g, are chosen from a Gaussian distribution, $P(g)$, of fixed mean, $\langle g \rangle$, and fixed standard deviation, σ_g. Here, σ_g represents the *strength* of the disorder, and each random value of g represents a *random parameter configuration* of the quantum spin model, describing a *random realization* of the system. For each random realization of the system, the quantity of interest, $Q(g)$, can be computed. A subsequent *quenched* average of $Q(g)$ over a statistically large number of random realizations is given by

$$\langle Q \rangle_d = \int P(g) Q(g) dg, \tag{90}$$

where the subscript d represents a quenched average, and $\langle Q \rangle$ is effectively a function of $\langle g \rangle$ and σ_g. Note that the corresponding *ordered* result can be obtained as a special case at $\sigma_g = 0$. Note also that disorder can, in principle, be present in a number of system parameters. In this paper, however, we confine ourselves in situations where only one chosen system parameter is disordered.

We start with the TXY model, choosing the field-strength h (and hence g, where J^{xy} is constant) to be the disordered system parameter. The quenched averaged LE, $\langle \langle E_{A_1A_2} \rangle \rangle_d$, and the bipartite entanglement, $\langle E_{A_1A_2:B} \rangle_d$, in the ground state of the system are numerically computed for different values of the disorder strength σ_g ($0.01 \leq \sigma_g \leq 0.1$), fixing $\langle g \rangle$ at similar values from the AFM and the PM phases of the model as the values of g in the ordered case. In each of these computations on an N-qubit system, both n and m are taken to be 1, similar to the ordered scenario. Our numerical data, exhibited in Fig. 8C. and fitted to Eq. (89) with $\lambda_0 = -0.36 \pm 0.024$, $\lambda_1 = 1.87 \pm 0.053$, and $\lambda_2 = -0.52 \pm 0.029$, indicate that the relation between $\langle E_{A_1A_2} \rangle$ and $E_{A_1A_2:B}$ is qualitatively robust against disorder in the field. Also, varying σ_g in the range $0.01 \leq \sigma_g \leq 0.1$ only changes the fitting parameters negligi-

bly. Similar analysis is performed for the XXZ model in an external field to arrive at a similar conclusion, where the data is fitted to Eq. (89) with $\lambda_0 = -0.26 \pm 0.093$, $\lambda_1 = 1.69 \pm 0.222$, and $\lambda_2 = -0.57 \pm 0.130$. See Fig. 8D.

V. CONCLUSIONS AND OUTLOOK

In this paper, we investigate dependence of the *gain* in the entanglement through localization over a group of qubits in a multi-qubit system via single-qubit projection measurements on the rest of the qubits on the amount of *loss* in bipartite entanglement during these measurements. We probe a number of paradigmatic N-qubit pure states, namely, the generalized GHZ, generalized W, Dicke, and the generalized Dicke states. We derive analytical bounds for the generalized GHZ and the generalized W states. We show that the gain is always equal to the loss in the former, while in the latter, lower and upper bounds of localizable entanglement can be derived in terms of the bipartite entanglement present in the system prior to the measurement process. In the case of the Dicke and the generalized Dicke states, a combination of analytical and numerical investigations reveal that the localizable entanglement tend to be equal to a component of the lost bipartite entanglement when the number of qubits increases. Modifications of these results, when the system is subjected to single-qubit Markovian and non-Markovian phase-flip channels, are also discussed. We extend our study to the ground states of the 1D quantum spin models, namely, the transverse-field XY model and the XXZ model in an external field, and numerically demonstrate a quadratic dependence of the localizable entanglement over the bipartite entanglement in the ground state prior to measurement, where measurement is restricted to one qubit only, and the entanglement is always computed in the 1:rest bipartition. This dependence is shown to be qualitatively robust even in the presence of disorder in the field strength.

A number of possible avenues of future research emerge from this study. Within the orbit of the results reported in this paper, it is important to understand how the results obtained in the case of the pure states are modified when different types of noise that are commonly occurring in experiments [94, 95], such as the bit-flip, depolarizing, and amplitude-damping [67, 68] noise are present in the system. However, investigating such noise channels may present new challenges in deriving the appropriate bounds, if any, on localizable entanglement. Also, in the case of the 1D quantum spin systems considered in this paper, it would be interesting to see the effect of the presence of disorder in the spin-spin interaction strengths along with a disordered field-strength. Besides, a plethora of quantum spin models are important from the perspective of quantum information theory [31, 32], and it is interesting to investigate whether a specific relation between the localized and the lost entanglement, similar to the one in the case of the models described in this study, exist in the ground states of these models in the presence and absence of disordered interactions, as well as in situations where the system is made open by allowing an interaction with the environment [96].

ACKNOWLEDGMENTS

We acknowledge the use of QIClib (https://github.com/titaschanda/QIClib) – a modern C++ library for general purpose quantum information processing and quantum computing.

Appendix A: Negativity

The amount of entanglement between two partitions A and B of a bipartite quantum state ρ_{AB} can be quantified by a bipartite entanglement measure [1, 2]. In this paper, we shall focus on negativity [56–60, 97] as a bipartite entanglement measure, which is defined as

$$E^{neg}_{A:B} = ||\rho^{T_B}_{AB}|| - 1, \tag{A1}$$

which corresponds to the absolute value of the sum of negative eigenvalues, λ, of $\rho^{T_B}_{AB}$, given by

$$E^{neg}_{A:B} = 2 \left| \sum_{\lambda_i < 0} \lambda_i \right|. \tag{A2}$$

Here, $||\varrho|| = \mathrm{Tr}\sqrt{\varrho^\dagger \varrho}$ is the trace norm of the density operator ϱ, computed as the sum of the singular values of ϱ. The matrix $\rho^{T_B}_{AB}$ is obtained by performing partial transposition of the density matrix ρ_{AB} with respect to the subsystem B. Since we only focus on negativity throughout this paper, we discard the superscript from $E^{neg}_{A:B}$, and denote the negativity between the partitions A and B simply by $E_{A:B}$.

Appendix B: Single- and two-qubit measurements

We first consider the single-qubit measurement in an N-qubit gW state, where (see Eq. (22))

$$f^0_0 = a_1 \mathrm{e}^{-\mathrm{i}\phi} \sin\frac{\theta}{2},\ f^1_0 = -a_1 \mathrm{e}^{-\mathrm{i}\phi} \cos\frac{\theta}{2}, \tag{B1}$$

$$f^0_i = a_{n+i} \cos\frac{\theta}{2},\ f^1_i = a_{n+i} \sin\frac{\theta}{2}, \tag{B2}$$

with $i = 1, 2, \cdots, N$, and

$$p_0 = a_1^2 \sin^2\frac{\theta}{2} + \cos^2\frac{\theta}{2} \sum_{i=2}^{N} a_i^2,$$
$$p_1 = a_1^2 \cos^2\frac{\theta}{2} + \sin^2\frac{\theta}{2} \sum_{i=2}^{N} a_i^2, \tag{B3}$$

such that $\langle \psi_k | \psi_k \rangle = 1$ for $k = 0, 1$. On the other hand, in the case of two-qubit projection measurements on an N-qubit gW state, the post-measured states are of the form given in Eq. (22), with the coefficients f^k_i as

$$f_0^0 = a_1 e^{-i\phi_1} \sin\frac{\theta_1}{2}\cos\frac{\theta_2}{2} + a_2 e^{-i\phi_2}\cos\frac{\theta_1}{2}\sin\frac{\theta_2}{2},\ f_0^1 = a_1 e^{-i\phi_1}\sin\frac{\theta_1}{2}\sin\frac{\theta_2}{2} - a_2 e^{-i\phi_2}\cos\frac{\theta_1}{2}\cos\frac{\theta_2}{2},$$
$$f_0^2 = -a_1 e^{-i\phi_1}\cos\frac{\theta_1}{2}\cos\frac{\theta_2}{2} + a_2 e^{-i\phi_2}\sin\frac{\theta_1}{2}\sin\frac{\theta_2}{2},\ f_0^3 = -a_1 e^{-i\phi_1}\cos\frac{\theta_1}{2}\sin\frac{\theta_2}{2} - a_2 e^{-i\phi_2}\sin\frac{\theta_1}{2}\cos\frac{\theta_2}{2}, \quad \text{(B4)}$$

and

$$f_i^0 = a_{n+i}\cos\frac{\theta_1}{2}\cos\frac{\theta_2}{2},\ f_i^1 = a_{n+i}\cos\frac{\theta_1}{2}\sin\frac{\theta_2}{2},\ f_i^2 = a_{n+i}\sin\frac{\theta_1}{2}\cos\frac{\theta_2}{2},\ f_i^3 = a_{n+i}\sin\frac{\theta_1}{2}\sin\frac{\theta_2}{2}, \quad \text{(B5)}$$

where $i = 1, 2, \cdots, N-n$, and the probabilities of obtaining the measurement outcome k, $k = 0, 1, 2, 3$, are given by

$$p_0 = a_1^2\sin^2\frac{\theta_1}{2}\cos^2\frac{\theta_2}{2} + a_2^2\cos^2\frac{\theta_1}{2}\sin^2\frac{\theta_2}{2} + \cos^2\frac{\theta_1}{2}\cos^2\frac{\theta_2}{2}\sum_{i=1}^{N-n} a_{n+i}^2,$$
$$p_1 = a_1^2\sin^2\frac{\theta_1}{2}\sin^2\frac{\theta_2}{2} + a_2^2\cos^2\frac{\theta_1}{2}\cos^2\frac{\theta_2}{2} + \cos^2\frac{\theta_1}{2}\sin^2\frac{\theta_2}{2}\sum_{i=1}^{N-n} a_{n+i}^2,$$
$$p_2 = a_1^2\cos^2\frac{\theta_1}{2}\cos^2\frac{\theta_2}{2} + a_2^2\sin^2\frac{\theta_1}{2}\sin^2\frac{\theta_2}{2} + \sin^2\frac{\theta_1}{2}\cos^2\frac{\theta_2}{2}\sum_{i=1}^{N-n} a_{n+i}^2,$$
$$p_3 = a_1^2\cos^2\frac{\theta_1}{2}\sin^2\frac{\theta_2}{2} + a_2^2\sin^2\frac{\theta_1}{2}\cos^2\frac{\theta_2}{2} + \sin^2\frac{\theta_1}{2}\sin^2\frac{\theta_2}{2}\sum_{i=1}^{N-n} a_{n+i}^2. \quad \text{(B6)}$$

For a three-qubit state belonging to the W class (see Eq. (47)), measurement on qubit 1 can be described in a way similar to that for the three-qubit gW state, with f_0^k $(k = 0, 1)$ given by

$$f_0^0 = a_0\cos\frac{\theta}{2} + a_1 e^{-i\phi}\sin\frac{\theta}{2},$$
$$f_0^1 = a_0\sin\frac{\theta}{2} - a_1 e^{-i\phi}\cos\frac{\theta}{2}, \quad \text{(B7)}$$

and $f_{1,2}^k$ $(k = 0, 1)$ given by

$$f_1^0 = a_2\cos\frac{\theta}{2},\quad f_2^0 = a_3\cos\frac{\theta}{2},$$
$$f_1^1 = a_2\sin\frac{\theta}{2},\quad f_2^1 = a_3\sin\frac{\theta}{2}, \quad \text{(B8)}$$

and

$$p_0 = \left|a_0\cos\frac{\theta}{2} + a_1 e^{-i\phi}\sin\frac{\theta}{2}\right|^2 + (a_2^2 + a_3^2)\cos^2\frac{\theta}{2},$$
$$p_1 = \left|a_0\sin\frac{\theta}{2} - a_1 e^{-i\phi}\cos\frac{\theta}{2}\right|^2 + (a_2^2 + a_3^2)\sin^2\frac{\theta}{2}. \quad \text{(B9)}$$

Appendix C: Specific examples

In this section, we demonstrate a number of results discussed in Secs. II and III using specific examples.

a. Upper bound for gW states. Consider the cases of $N = 3, 4$, for which the family of states providing the upper bound of $\langle E_{A_1A_2}\rangle$ in the case of gW states with real coefficients can be written as

$$|\Psi_3\rangle = a|100\rangle + \sqrt{\frac{1-a^2}{2}}(|010\rangle + |001\rangle), \quad \text{(C1)}$$
$$|\Psi_4\rangle = a|1000\rangle + \sqrt{\frac{1-a^2}{2}}|0100\rangle + b|0010\rangle + \sqrt{\frac{1-a^2-2b^2}{2}}|0001\rangle, \quad \text{(C2)}$$

where a, b are real numbers. The behaviour of $\langle E_{A_1A_2}\rangle$ as a function of a, b is shown in Figs. 2A. and B. Also, $\langle E_{A_1A_2}\rangle$ for the state $|\Psi_3\rangle$ provides an upper bound for $\langle E_{A_1A_2}\rangle$ corresponding to all three-qubit gW states with complex coefficients. This is demonstrated by the $\langle E_{A_1A_2}\rangle$ values corresponding to 10^6 Haar-uniformly generated three-qubit gW states lying below the upper bound.

b. Maximum bipartite entanglement for gW states. The line $E_{A_1A_2:B} = 1$ corresponds to the family of states given by

$$\sum_{i\in B} a_i^2 = \left(4\sum_{i\in A} a_i^2\right)^{-1}. \quad \text{(C3)}$$

Specifically, for a three-qubit system, this family is given by

$$|\Phi_3\rangle = \sqrt{\frac{1}{2}}|100\rangle + a|010\rangle + \sqrt{\frac{1}{2} - a^2}|001\rangle, \quad \text{(C4)}$$

while for $N = 4$, $n = m = 1$,

$$|\Phi_4\rangle = \sqrt{\frac{1}{2}}|1000\rangle + a|0100\rangle + b|0010\rangle + \sqrt{\frac{1}{2} - a^2 - b^2}|0001\rangle. \quad \text{(C5)}$$

[1] Ryszard Horodecki, Paweł Horodecki, Michał Horodecki, and Karol Horodecki, "Quantum entanglement," Rev. Mod. Phys. **81**, 865–942 (2009).

[2] Otfried Gühne and Géza Tóth, "Entanglement detection," Phys. Rep. **474**, 1–75 (2009).

[3] Charles H. Bennett, Gilles Brassard, Claude Crépeau, Richard Jozsa, Asher Peres, and William K. Wootters, "Teleporting an unknown quantum state via dual classical and einstein-podolsky-rosen channels," Phys. Rev. Lett. **70**, 1895–1899 (1993).

[4] Dik Bouwmeester, Jian-Wei Pan, Klaus Mattle, Manfred Eibl, Harald Weinfurter, and Anton Zeilinger, "Experimental quantum teleportation," Nature **390**, 575–579 (1997).

[5] Charles H. Bennett and Stephen J. Wiesner, "Communication via one- and two-particle operators on einstein-podolsky-rosen states," Phys. Rev. Lett. **69**, 2881–2884 (1992).

[6] Klaus Mattle, Harald Weinfurter, Paul G. Kwiat, and Anton Zeilinger, "Dense coding in experimental quantum communication," Phys. Rev. Lett. **76**, 4656–4659 (1996).

[7] Aditi Sen(De) and Ujjwal Sen, "Quantum advantage in communication networks," Phys. News **40**, 17–32 (2011), arXiv:1105.2412.

[8] Artur K. Ekert, "Quantum cryptography based on bell's theorem," Phys. Rev. Lett. **67**, 661–663 (1991).

[9] Thomas Jennewein, Christoph Simon, Gregor Weihs, Harald Weinfurter, and Anton Zeilinger, "Quantum cryptography with entangled photons," Phys. Rev. Lett. **84**, 4729–4732 (2000).

[10] Veronika E Hubeny, "The AdS/CFT correspondence," Classical Quant. Grav. **32**, 124010 (2015).

[11] Fernando Pastawski, Beni Yoshida, Daniel Harlow, and John Preskill, "Holographic quantum error-correcting codes: toy models for the bulk/boundary correspondence," J. High. Energy Phys. **2015**, 149 (2015).

[12] Ahmed Almheiri, Xi Dong, and Daniel Harlow, "Bulk locality and quantum error correction in ads/cft," J. High Energy Phys. **4**, 163 (2015).

[13] A. Jahn, M. Gluza, F. Pastawski, and J. Eisert, "Holography and criticality in matchgate tensor networks," arXiv:1711.03109 (2017).

[14] Don N. Page and William K. Wootters, "Evolution without evolution: Dynamics described by stationary observables," Phys. Rev. D **27**, 2885–2892 (1983).

[15] Rodolfo Gambini, Rafael A. Porto, Jorge Pullin, and Sebastián Torterolo, "Conditional probabilities with dirac observables and the problem of time in quantum gravity," Phys. Rev. D **79**, 041501 (2009).

[16] Ekaterina Moreva, Giorgio Brida, Marco Gramegna, Vittorio Giovannetti, Lorenzo Maccone, and Marco Genovese, "Time from quantum entanglement: An experimental illustration," Phys. Rev. A **89**, 052122 (2014).

[17] Neill Lambert, Yueh-Nan Chen, Yuan Chung Cheng, Che-Ming Li, Guang Yin Chen, and Franco Nori, "Quantum biology," Nat. Phys. **9**, 10–18 (2013).

[18] J. M. Raimond, M. Brune, and S. Haroche, "Manipulating quantum entanglement with atoms and photons in a cavity," Rev. Mod. Phys. **73**, 565–582 (2001).

[19] R. Prevedel, G. Cronenberg, M. S. Tame, M. Paternostro, P. Walther, M. S. Kim, and A. Zeilinger, "Experimental realization of dicke states of up to six qubits for multiparty quantum networking," Phys. Rev. Lett. **103**, 020503 (2009).

[20] Stefanie Barz, "Quantum computing with photons: introduction to the circuit model, the one-way quantum computer, and the fundamental principles of photonic experiments," J. Phys. B **48**, 083001 (2015).

[21] D. Leibfried, R. Blatt, C. Monroe, and D. Wineland, "Quantum dynamics of single trapped ions," Rev. Mod. Phys. **75**, 281–324 (2003).

[22] D. Leibfried, E. Knill, S. Seidelin, J. Britton, R. B. Blakestad, J. Chiaverini, D. B. Hume, W. M. Itano, J. D. Jost, C. Langer, R. Ozeri, R. Reichle, and D. J. Wineland, "Creation of a six-atom 'schrödinger cat' state," Nature **438**, 639–642 (2005).

[23] Kenneth R. Brown, Jungsang Kim, and Christopher Monroe, "Co-designing a scalable quantum computer with trapped atomic ions," Nature Phys. J. Quant. Inf. **2**, 16034 EP – (2016).

[24] Olaf Mandel, Markus Greiner, Artur Widera, Tim Rom, Theodor W. Hansch, and Immanuel Bloch, "Controlled collisions for multi-particle entanglement of optically trapped atoms," Nature **425**, 937–940 (2003).

[25] Immanuel Bloch, "Exploring quantum matter with ultracold atoms in optical lattices," J. Phys. B: At. Mol. Opt. Phys. **38**, S629–S643 (2005).

[26] Immanuel Bloch, Jean Dalibard, and Wilhelm Zwerger, "Many-body physics with ultracold gases," Rev. Mod. Phys. **80**, 885–964 (2008).

[27] John Clarke and Frank K. Wilhelm, "Superconducting quantum bits," Nature **453**, 1031–1042 (2008).

[28] R. Barends, J. Kelly, A. Megrant, A. Veitia, D. Sank, E. Jeffrey, T. C. White, J. Mutus, A. G. Fowler, B. Campbell, Y. Chen, Z. Chen, B. Chiaro, A. Dunsworth, C. Neill, P. O'Malley, P. Roushan, A. Vainsencher, J. Wenner, A. N. Korotkov, A. N. Cleland, and John M. Martinis, "Superconducting quantum circuits at the surface code threshold for fault tolerance," Nature **508**, 500 (2014).

[29] C. Negrevergne, T. S. Mahesh, C. A. Ryan, M. Ditty, F. Cyr-Racine, W. Power, N. Boulant, T. Havel, D. G. Cory, and R. Laflamme, "Benchmarking quantum control methods on a 12-qubit system," Phys. Rev. Lett. **96**, 170501 (2006).

[30] R. Augusiak, F. M. Cucchietti, and M. Lewenstein, "Many-body physics from a quantum information perspective," in *Modern Theories of Many-Particle Systems in Condensed Matter Physics*, edited by Daniel C. Cabra, Andreas Honecker, and Pierre Pujol (Springer Berlin Heidelberg, Berlin, Heidelberg, 2012) pp. 245–294.

[31] Luigi Amico, Rosario Fazio, Andreas Osterloh, and Vlatko Vedral, "Entanglement in many-body systems," Rev. Mod. Phys. **80**, 517–576 (2008).

[32] Gabriele De Chiara and Anna Sanpera, Reports on Progress in Physics **81**, 074002 (2018).

[33] Michał Horodecki, "Entanglement measures," Quantum Inf. Comput. **1**, 3–26 (2001).

[34] D. M. Greenberger, M. A. Horne, and A. Zeilinger, *Bell's theorem, quantum theory and conceptions of the universe* (Kluwer, Netherlands, 1989).

[35] M Hein, W Dür, Jens Eisert, Robert Raussendorf, M Van den Nest, and H J. Briegel, "Entanglement in graph states and its applications," arXiv:quant-ph/0602096 (2006).

[36] Robert Raussendorf, Daniel E. Browne, and Hans J. Briegel, "Measurement-based quantum computation on cluster states," Phys. Rev. A **68**, 022312 (2003).

[37] Keisuke Fujii, "Quantum computation with topological codes: from qubit to topological fault-tolerance," arXiv:1504.01444 (2015).

[38] D. P. DiVincenzo, C. A. Fuchs, H. Mabuchi, J. A. Smolin, A. Thapliyal, and A. Uhlmann, "Entanglement of assistance,"

arXiv:quant-ph/9803033 (1998).
[39] F. Verstraete, M. Popp, and J. I. Cirac, "Entanglement versus correlations in spin systems," Phys. Rev. Lett. **92**, 027901 (2004).
[40] F. Verstraete, M. A. Martín-Delgado, and J. I. Cirac, "Diverging entanglement length in gapped quantum spin systems," Phys. Rev. Lett. **92**, 087201 (2004).
[41] M. Popp, F. Verstraete, M. A. Martín-Delgado, and J. I. Cirac, "Localizable entanglement," Phys. Rev. A **71**, 042306 (2005).
[42] Debasis Sadhukhan, Sudipto Singha Roy, Amit Kumar Pal, Debraj Rakshit, Aditi Sen(De), and Ujjwal Sen, "Multipartite entanglement accumulation in quantum states: Localizable generalized geometric measure," Phys. Rev. A **95**, 022301 (2017).
[43] David Amaro, Markus Müller, and Amit Kumar Pal, "Estimating localizable entanglement from witnesses," New J. Phys. **20**, 063017 (2018).
[44] David Amaro, Markus Müller, and Amit Kumar Pal, "Scalable characterization of localizable entanglement in noisy topological quantum codes," New Journal of Physics **22**, 053038 (2020).
[45] B.-Q. Jin and V. E. Korepin, "Localizable entanglement in antiferromagnetic spin chains," Phys. Rev. A **69**, 062314 (2004).
[46] Stein Olav Skrøvseth and Stephen D. Bartlett, "Phase transitions and localizable entanglement in cluster-state spin chains with ising couplings and local fields," Phys. Rev. A **80**, 022316 (2009).
[47] Pietro Smacchia, Luigi Amico, Paolo Facchi, Rosario Fazio, Giuseppe Florio, Saverio Pascazio, and Vlatko Vedral, "Statistical mechanics of the cluster ising model," Phys. Rev. A **84**, 022304 (2011).
[48] Sebastián Montes and Alioscia Hamma, "Phase diagram and quench dynamics of the cluster-xy spin chain," Phys. Rev. E **86**, 021101 (2012).
[49] Antonio Acín, J. Ignacio Cirac, and Maciej Lewenstein, "Entanglement percolation in quantum networks," Nat. Phys. **3**, 256 (2007).
[50] Sandu Popescu and Daniel Rohrlich, "Thermodynamics and the measure of entanglement," Phys. Rev. A **56**, R3319–R3321 (1997).
[51] V. Vedral and M. B. Plenio, "Entanglement measures and purification procedures," Phys. Rev. A **57**, 1619–1633 (1998).
[52] Guifré Vidal, "Entanglement monotones," Journal of Modern Optics **47**, 355–376 (2000).
[53] John A. Smolin, Frank Verstraete, and Andreas Winter, "Entanglement of assistance and multipartite state distillation," Phys. Rev. A **72**, 052317 (2005).
[54] Dong Yang and Jens Eisert, "Entanglement combing," Phys. Rev. Lett. **103**, 220501 (2009).
[55] Klée Pollock, Ge Wang, and Eric Chitambar, "Entanglement of assistance in three-qubit systems," Phys. Rev. A **103**, 032428 (2021).
[56] Asher Peres, "Separability criterion for density matrices," Phys. Rev. Lett. **77**, 1413–1415 (1996).
[57] Michal Horodecki, Pawel Horodecki, and Ryszard Horodecki, "Separability of mixed states: necessary and sufficient conditions," Phys. Lett. A **223**, 1 – 8 (1996).
[58] G. Vidal and R. F. Werner, "Computable measure of entanglement," Phys. Rev. A **65**, 032314 (2002).
[59] Karol Życzkowski, Paweł Horodecki, Anna Sanpera, and Maciej Lewenstein, "Volume of the set of separable states," Phys. Rev. A **58**, 883–892 (1998).
[60] Jinhyoung Lee, M. S. Kim, Y. J. Park, and S. Lee, "Partial teleportation of entanglement in a noisy environment," Journal of Modern Optics **47**, 2151–2164 (2000).
[61] W. Dür, G. Vidal, and J. I. Cirac, "Three qubits can be entangled in two inequivalent ways," Phys. Rev. A **62**, 062314 (2000).
[62] Aditi Sen(De), Ujjwal Sen, Marcin Wieśniak, Dagomir Kaszlikowski, and Marek Żukowski, "Multiqubit w states lead to stronger nonclassicality than greenberger-horne-zeilinger states," Phys. Rev. A **68**, 062306 (2003).
[63] R. H. Dicke, "Coherence in spontaneous radiation processes," Phys. Rev. **93**, 99–110 (1954).
[64] Marcel Bergmann and Otfried Gühne, "Entanglement criteria for dicke states," Journal of Physics A: Mathematical and Theoretical **46**, 385304 (2013).
[65] Bernd Lücke, Jan Peise, Giuseppe Vitagliano, Jan Arlt, Luis Santos, Géza Tóth, and Carsten Klempt, "Detecting multiparticle entanglement of dicke states," Phys. Rev. Lett. **112**, 155304 (2014).
[66] Asutosh Kumar, Himadri Shekhar Dhar, R. Prabhu, Aditi Sen(De), and Ujjwal Sen, "Forbidden regimes in the distribution of bipartite quantum correlations due to multiparty entanglement," Physics Letters A **381**, 1701–1709 (2017).
[67] M. A. Nielsen and I. L. Chuang, *Quantum Computation and Quantum Information* (Cambridge University Press, 2010).
[68] A. S. Holevo and V. Giovannetti, "Quantum channels and their entropic characteristics," Rep. Prog. Phys. **75**, 046001 (2012).
[69] Ting Yu and J. H. Eberly, "Sudden death of entanglement," Science **323**, 598–601 (2009), https://science.sciencemag.org/content/323/5914/598.full.pdf.
[70] Sonja Daffer, Krzysztof Wódkiewicz, James D. Cresser, and John K. McIver, "Depolarizing channel as a completely positive map with memory," Phys. Rev. A **70**, 010304 (2004).
[71] U. Shrikant, R. Srikanth, and Subhashish Banerjee, "Non-markovian dephasing and depolarizing channels," Phys. Rev. A **98**, 032328 (2018).
[72] Ribhu Gupta, Shashank Gupta, Shiladitya Mal, Aditi Sen(De), and Ujjwal Sen, "Constructive feedback of non-markovianity on resources in random quantum states," arXiv:2005.04009 (2020).
[73] Cirano De Dominicis and Irene Giardina, *Random Fields and Spin Glasses: A Field Theory Approach* (Cambridge University Press, 2006).
[74] E. Lieb, T. Schultz, and D. Mattis, "Two soluble models of an antiferromagnetic chain," Annals of Physics **16**, 407–466 (1961).
[75] E. Barouch, B. M. McCoy, and M. Dresden, "Statistical mechanics of the XY model. I," Phys. Rev. A **2**, 1075–1092 (1970).
[76] E. Barouch and B. M. McCoy, "Statistical mechanics of the XY model. II. spin-correlation functions," Phys. Rev. A **3**, 786–804 (1971).
[77] E. Barouch and B. M. McCoy, "Statistical mechanics of the XY model. III," Phys. Rev. A **3**, 2137–2140 (1971).
[78] Bikas K Chakrabarti, Amit Dutta, and Parongama Sen, *Quantum Ising Phases and Transitions in Transverse Ising Models*, Vol. 41 (Springer, Heidelberg, 1996).
[79] Subir Sachdev, *Quantum Phase Transitions*, 2nd ed. (Cambridge University Press, 2011).
[80] C. N. Yang and C. P. Yang, "One-dimensional chain of anisotropic spin-spin interactions. i. proof of bethe's hypothesis for ground state in a finite system," Phys. Rev. **150**, 321–327 (1966).
[81] C. N. Yang and C. P. Yang, "One-dimensional chain of anisotropic spin-spin interactions. ii. properties of the ground-state energy per lattice site for an infinite system," Phys. Rev. **150**, 327–339 (1966).
[82] C. N. Yang and C. P. Yang, "One-dimensional chain of anisotropic spin-spin interactions. iii. applications," Phys. Rev. **151**, 258–264 (1966).

[83] A. Langari, "Phase diagram of the antiferromagnetic xxz model in the presence of an external magnetic field," Phys. Rev. B **58**, 14467–14475 (1998).

[84] Hans-Jürgen Mikeska and Alexei K. Kolezhuk, "One-dimensional magnetism," in *Quantum Magnetism*, edited by Ulrich Schollwöck, Johannes Richter, Damian J. J. Farnell, and Raymod F. Bishop (Springer Berlin Heidelberg, Berlin, Heidelberg, 2004) pp. 1–83.

[85] T. Giamarchi, *Quantum physics in one dimension*, International series of monographs on physics (Clarendon Press, Oxford, 2004).

[86] Ingemar Bengtsson and Karol Zyczkowski, *Geometry of Quantum States: An Introduction to Quantum Entanglement* (Cambridge University Press, 2006).

[87] Ratul Banerjee, Amit Kumar Pal, and Aditi Sen(De), "Uniform decoherence effect on localizable entanglement in random multiqubit pure states," Phys. Rev. A **101**, 042339 (2020).

[88] Xiao-yu Chen and Li-zhen Jiang, "Noise tolerance of dicke states," Phys. Rev. A **101**, 012308 (2020).

[89] Anna Sanpera, Rolf Tarrach, and Guifré Vidal, "Local description of quantum inseparability," Phys. Rev. A **58**, 826–830 (1998).

[90] Swapan Rana, "Negative eigenvalues of partial transposition of arbitrary bipartite states," Phys. Rev. A **87**, 054301 (2013).

[91] P. Pfeuty, "The one-dimensional Ising model with a transverse field," Annals of Physics **57**, 79–90 (1970).

[92] A. Osterloh, Luigi Amico, G. Falci, and Rosario Fazio, "Scaling of entanglement close to a quantum phase transition," Nature **416**, 608–610 (2002).

[93] Tobias J. Osborne and Michael A. Nielsen, "Entanglement in a simple quantum phase transition," Phys. Rev. A **66**, 032110 (2002).

[94] Philipp Schindler, Daniel Nigg, Thomas Monz, Julio T Barreiro, Esteban Martinez, Shannon X Wang, Stephan Quint, Matthias F Brandl, Volckmar Nebendahl, Christian F Roos, Michael Chwalla, Markus Hennrich, and Rainer Blatt, "A quantum information processor with trapped ions," New Journal of Physics **15**, 123012 (2013).

[95] A. Bermudez, X. Xu, R. Nigmatullin, J. O'Gorman, V. Negnevitsky, P. Schindler, T. Monz, U. G. Poschinger, C. Hempel, J. Home, F. Schmidt-Kaler, M. Biercuk, R. Blatt, S. Benjamin, and M. Müller, "Assessing the progress of trapped-ion processors towards fault-tolerant quantum computation," Phys. Rev. X **7**, 041061 (2017).

[96] H.-P. Breuer and F. Petruccione, *The Theory of Open Quantum Systems* (Oxford University Press, Oxford, 2002).

[97] M. B. Plenio, "Logarithmic negativity: A full entanglement monotone that is not convex," Phys. Rev. Lett. **95**, 090503 (2005).